Human Molecular Genetics, 2014, Vol. 23, No. 1 **52–68**
doi:10.1093/hmg/ddt395
Advance Access published on August 13, 2013

Mouse genetics and proteomic analyses demonstrate a critical role for complement in a model of DHRD/ML, an inherited macular degeneration

Donita L. Garland[1,*], Rosario Fernandez-Godino[1], Inderjeet Kaur[3], Kaye D. Speicher[4], James M. Harnly[5], John D. Lambris[6], David W. Speicher[4] and Eric A. Pierce[1,2,*]

[1]Ocular Genomics Institute and [2]Berman-Gund Laboratory for the Study of Retinal Degenerations, Department of Ophthalmology, Massachusetts Eye and Ear Infirmary, Harvard Medical School, Boston, MA, USA [3]Kallam Anji Reddy Molecular Genetics Laboratory, LV Prasad Eye Institute (LVPEI), Kallam Anji Reddy Campus, LV Prasad Marg, Hyderabad, India [4]Center for Systems and Computational Biology and Molecular Oncogenesis Program, The Wistar Institute, Philadelphia, PA, USA [5]Food Composition and Methods Development Laboratory, Beltsville Human Nutrition Research Center, U.S. Department of Agriculture, Beltsville, MD, USA [6]Department of Pathology and Laboratory Medicine, University of Pennsylvania Perelman School of Medicine, Philadelphia, PA, USA

Received May 31, 2013; Revised July 24, 2013; Accepted August 6, 2013

Macular degenerations, inherited and age related, are important causes of vision loss. Human genetic studies have suggested perturbation of the complement system is important in the pathogenesis of age-related macular degeneration. The mechanisms underlying the involvement of the complement system are not understood, although complement and inflammation have been implicated in drusen formation. Drusen are an early clinical hallmark of inherited and age-related forms of macular degeneration. We studied one of the earliest stages of macular degeneration which precedes and leads to the formation of drusen, i.e. the formation of basal deposits. The studies were done using a mouse model of the inherited macular dystrophy Doyne Honeycomb Retinal Dystrophy/Malattia Leventinese (DHRD/ML) which is caused by a p.Arg345Trp mutation in *EFEMP1*. The hallmark of DHRD/ML is the formation of drusen at an early age, and gene targeted *Efemp1*$^{R345W/R345W}$ mice develop extensive basal deposits. Proteomic analyses of Bruch's membrane/choroid and Bruch's membrane in the *Efemp1*$^{R345W/R345W}$ mice indicate that the basal deposits comprise normal extracellular matrix (ECM) components present in abnormal amounts. The proteomic analyses also identified significant changes in proteins with immune-related function, including complement components, in the diseased tissue samples. Genetic ablation of the complement response via generation of *Efemp1*$^{R345W/R345W}$:*C3*$^{-/-}$ double-mutant mice inhibited the formation of basal deposits. The results demonstrate a critical role for the complement system in basal deposit formation, and suggest that complement-mediated recognition of abnormal ECM may participate in basal deposit formation in DHRD/ML and perhaps other macular degenerations.

INTRODUCTION

Macular degenerations are important causes of vision loss. Inherited macular degenerations often affect individuals in the first two decades of life (1). Age-related macular degeneration (AMD) is the leading cause of vision loss in individuals over 65 years of age in the Western world and is increasing in prevalence in other parts of the world (2–5). AMD is a complex disorder with age as the major risk factor (6,7). Genetics and other factors such as smoking, hypertension, obesity and diet also contribute to the risk of the disease (6,8–10). Genetic association studies have identified 19 loci that are associated with the risk of developing AMD (11). These loci include genes involved with lipid metabolism, angiogensis, extracellular matrix (ECM)

*To whom correspondence should be addressed at: Ocular Genomics Institute, Department of Ophthalmology, Massachusetts Eye and Ear Infirmary, Harvard Medical School, 243 Charles Street, Boston, MA 02114, USA. Email: donita_garland@meei.harvard.edu (D.L.G.); Email: eric_pierce@meei.harvard.edu (E.A.P.)

remodeling and the complement system. Variants of complement genes and the *ARMS2/HTRA1* locus on chromosome 10q26, account for the majority of the genetic risk for AMD (7,11).

Human genetic studies identified variants in genes for complement factor H (*CFH*), complement C3 (*C3*), complement C2 (*C2*), complement factor B (*CFB*), complement factor D (*CFD*) and complement factor I (*CFI*) that alter the risk of AMD or the progression to advanced AMD (10,12–23). The complement system can be activated through three major pathways: classical, lectin and alternative pathways (24,25). Complement C3 is central to all three pathways. C2 is a component of the classical and lectin pathways and CFB, CFH and CFD are components of the alternative pathway. It is not known which complement pathway initiates the involvement of complement in AMD or whether more than one pathway is involved. The link between AMD and variants of CFH, a regulator of the alternative pathway, seems to be stronger than that of the other complement proteins, suggesting that the alternative pathway may be the major pathway involved (12–15). The specific mechanisms by which complement contributes to the pathogenesis of AMD are not known. It is, also, not known if complement has a major role in the pathogenesis of inherited macular degenerations. An inhibitor of the activation of complement C3 leads to a regression of drusen in nonhuman primates (26). Drugs have been designed and some are in trials that target additional complement components as a way of limiting inflammation which is thought to be a major factor in drusen formation and AMD pathogenesis (27–30).

The presence of drusen is one of the first clinical indicators of a risk for developing macular degeneration and a characteristic clinical finding in the maculae of patients with both age-related and inherited macular degenerations (31,32). Drusen are extracellular accumulations of proteins and lipid between the retinal pigment epithelia (RPE) and Bruch's membrane (BrM) (33–35). Many components of drusen have been identified, but the sources of these components and the mechanisms of drusen formation are not fully understood (27,36–46). The presence of complement proteins in drusen led to the original hypothesis that the immune system and inflammation were involved (27,28). The location of drusen between the RPE and BrM suggests that the components may be primarily derived from the RPE, but there is evidence that choroid and possibly the retina may also contribute to drusen formation (45,47).

Basal deposits, microscopic accumulations of material under the RPE, have been implicated as precursors to drusen and as indicators of risk for developing AMD (33,35,48–50). The mechanisms involved in the formation of basal deposits are, however, not understood. Basal laminar deposits were reported to contain long-spaced collagen, carbohydrate structures, laminin, fibronectin, collagen type IV and vesicles (51,52). Studies of AMD patients and studies on transgenic mice suggest a role of lipid metabolism and high-fat diets in basal deposit formation (40,43,53). It is known that several genetically engineered mouse strains used to study AMD, each with a different targeted gene, develop basal deposits (54–59). Thus, there may be common mechanisms involved in deposit formation.

We investigated the formation of basal deposits using an animal model of the inherited macular dystrophy, Doyne Honeycomb Retinal Dystrophy/Malattia Leventinese (DHRD/ML) (60). DHRD/ML is the inherited macular dystrophy that is phenotypically most similar to the more common AMD (57,61,62). A hallmark of DHRD/ML is extensive drusen which can be present as early as the second decade of life (60). DHRD/ML is caused by a p.Arg345Trp mutation in epidermal growth factor-containing fibulin-like extracellular matrix protein 1 (EFEMP1) (56,63).

EFEMP1, also known as fibulin 3, is a member of the fibulin family of seven extracellular matrix proteins (64–67). Variants in *FBLN5* (fibulin 5), but not in *EFEMP1*, have been associated with the risk of AMD (61). EFEMP1 is ubiquitously expressed in epithelial and endothelial cells and is a component of BrM (64,66–68). EFEMP1 has been shown to have a role in elastic fiber integrity, in signal transduction by binding and activating EGF receptors and in altering tumor growth by modulating the extracellular environment (67,69–72). In addition, EFEMP1 is a binding partner of TIMP3 which, when mutated, causes the inherited Sorsby's fundus dystrophy (73,74).

Gene targeted mice ($Efemp1^{R345W/R345W}$) develop features of macular degeneration including the formation of extensive basal deposits with age and RPE abnormalities including vacuoles and loss of basolateral infoldings (56,58). These are the result of the p.Arg345Trp mutation in *Efemp1* as *Efemp1* knock-out mice do not have a retinal phenotype (69). Increased levels of complement C3 between the RPE and BrM were present in the mutant mice implicating the complement system in the pathology of the mutation in *Efemp1* (56). Thus, the $Efemp1^{R345W/R345W}$ knock-in mice provide a useful model for studying the formation of basal deposits as potential precursors to drusen formation and the potential involvement of the complement system.

In this study, we used two approaches, proteomics and mouse genetics, to investigate basal deposit formation and the role that the complement system may have in this process in the $Efemp1^{R345W/R345W}$ mice. The proteomics analyses of BrM and the Bruch's membrane/choroid (BrCh) of mutant and control mice further implicate complement and immune processes in the pathogenesis of the p.Arg345Trp mutation in *Efemp1*. The genetic studies functionally validated a critical role for complement in the formation of basal deposits in the $Efemp1^{R345W/R345W}$ mice.

RESULTS

Proteomic analyses

The mechanisms of basal deposit formation in the $Efemp1^{R345W/R345W}$ mice were investigated by analyzing the proteins in BrCh and BrM using mass spectrometry. BrCh from 8, 14 and 24 month old mice was analyzed in order to follow protein changes during the time that the basal deposits have formed (8 months) until the time they are extensive and can be a few microns thick (24 months) (56,58). BrM samples (24 months) were analyzed to more specifically investigate the composition of the basal deposits, as the deposits remained with BrM after the removal of the RPE cells (Fig. 1). The numbers of proteins identified for each of the eight samples studied are listed in Table 1. A total of 1062 proteins were identified among the eight samples. Fifty percent of these proteins were present in at least seven of the eight samples. Complete lists of the proteins identified and estimates of their abundances based on normalized spectral counts for each protein are

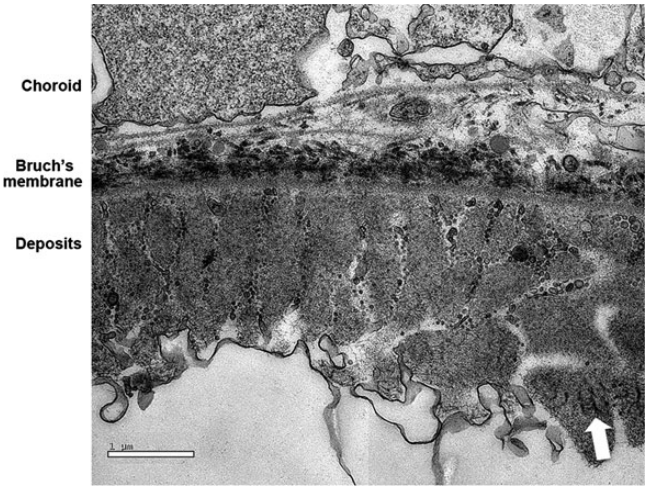

Figure 1. Electron micrograph of basal deposits associated with BrM after the removal of RPE cells as described in Materials and Methods. Wide-spaced collagen is indicated by the white arrow.

Table 1. Number of proteins identified in each sample

Age (months)	Sample	Mice	Number
8	BrCh	*Efemp1*-R345W	844
8	BrCh	wt	824
14	BrCh	*Efemp1*-R345W	889
14	BrCh	wt	913
24	BrCh	*Efemp1*-R345W	795
24	BrCh	wt	654
24	BrM	*Efemp1*-R345W	727
24	BrM	wt	606
Total number of proteins identified in all samples			1062
Number of proteins identified in seven of eight samples			530

included in Supplementary Material, Table S1. Normalized spectral counts provide a reliable estimate of the relative abundance of proteins detected by LC–MS/MS analyses (75,76). The amount of protein analyzed in each sample was comparable and this is evidenced by the similarity of the relative abundances for the majority of proteins across the samples.

Supplementary Material, Table S2 contains the list of 66 ECM and ECM-associated proteins identified in 24 months BrM, their abundance and the ratios between mutant and wild–type (wt) samples. They include 34 ECM proteoglycans, 13 collagens, 7 proteoglycans, 7 ECM affiliated proteins and 5 ECM regulatory proteins (77,78). These categories are identified in Supplementary Material, Table S2. Following these is a list of integrins and all other proteins identified in BrM, their abundances and the ratios of the abundance in mutant relative to wt mice.

The most abundant components of the wt BrM include collagens, vimentin, perlecan, lumican, laminins, and the matricellular proteins, decorin, biglycan, nidogen 1 and nidogen 2. The most abundant collagens present are types VI, XII, I and XVIII. Collagen type IV, a component of basal lamina, is present at lower abundance. Elastin was not detected in BrM. Elastin becomes cross-linked but even in the absence of cross-linking there are very few tryptic peptides from elastin that could have been detected by mass spectrometry in these experiments (79).

Identification of proteins associated with the mutant phenotype

Principal component analysis

Principal component analysis (PCA) was used to analyze the normalized spectral counts for the eight sets of data listed in Supplemental Material, Table S1 (8, 14, 24 months for BrCh and 24 months for BrM) to determine the relationships among these sets of data. PCA is an exploratory method that makes no a priori decisions about the relationships among the data (80). The correlated multivariate data are reduced to uncorrelated variables, called the principal components (PCs), based on the variance of the data. The general trends in a data set can usually be seen in plots of the first two or three PCs. The contributions of each protein to the PCs are obtained from their respective PCA loadings (81). PCA is now frequently used to analyze proteomic data (82,83).

A PCA scores plot for the eight sets of data is shown in Figure 2A. PC1 (*x*-axis) accounts for 31% of the variance and is roughly correlated with the age of the mice. An additional 21% of the variance is accounted for by PC2 (*y*-axis) and is correlated with the mouse genetics (wt versus *Efemp1*$^{R345W/R345W}$ mice) for the 24 months mice. Simplistically, the distance between data points provides a relative measure of similarity among the data sets, with closer data points being more similar. The plot clearly shows that at 8 months there is little effect of the mutation in *Efemp1* on the proteins in BCh samples. The effect of the mutation begins to be apparent by 14 months as the distance between the data points is slightly greater. At 24 months, the difference between the samples from mutant and wt mice is pronounced. There is a wide separation between the data points for the mutant and the wt mice for both the BCh samples and the BrM samples. PC2 is highly correlated with the difference between the wt and mutant mice at 24 months and, thus, is most associated with the basal deposit phenotype.

The proteins most responsible for differentiation with respect to age (PC1) and genetics (PC2) based on the loadings are listed in Tables 2 and 3. Each list in Tables 2 and 3 contains the top 60 proteins that contribute the most and account for about half of the variance in PC1 and in PC2 (see Materials and Methods and Supplementary Material, Fig. S1).

Hierarchical cluster analysis

Hierarchical cluster analysis (HCA) using a standard clustering algorithm (K nearest neighbor) was performed as an additional approach to verify the relationships among the sets of data (Fig. 2B) (84). The observed pattern for HCA agrees with that found using PCA. The 8 months samples (mutant and wt) and the 14 months samples (mutant and wt) are linked first to each other indicating a high degree of similarity. At 24 months, the mutant BCh and BrM samples were linked, indicating that they are more similar to each other than to their respective wt samples, confirming that the basal deposits altered protein composition most at 24 months of age.

Matched pair analysis

Matched pair analysis was also used to identify biologically significant protein changes associated with the development of basal deposits in the *Efemp1*$^{R345W/R345W}$ mice (85). This

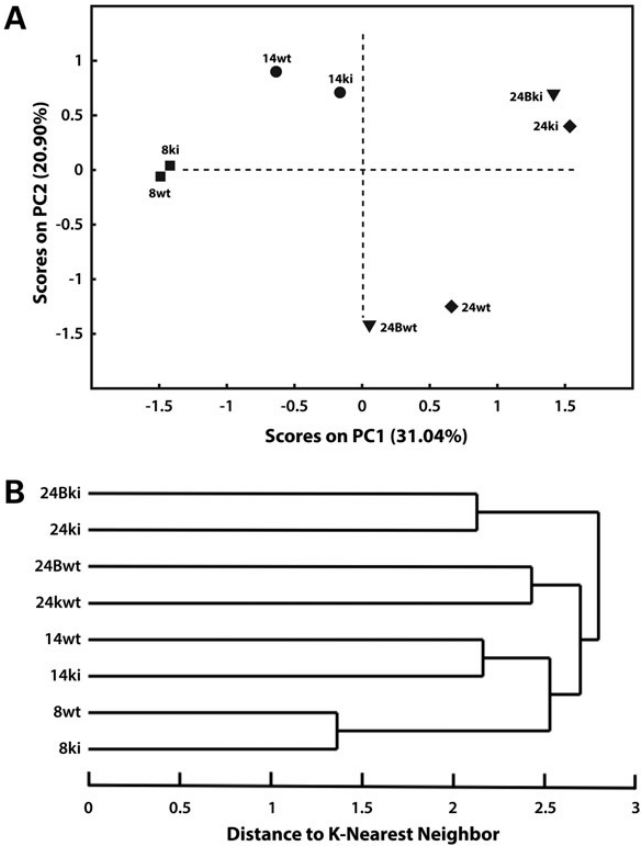

Figure 2. Principal component and hierarchical cluster analyses of proteomic data. (**A**) PCA of normalized spectral count data for the eight sets of proteomic data listed in Table 1 and Supplementary Material, Table S1. The distance between the data points reflects the similarity of the data sets, i.e. the closer the data points the more similar the data sets. As indicated, the two strongest contributors to differences in the proteins detected in the mutant and control samples were age (PC1, *x*-axis) and genetics (PC2, *y*-axis). The wt and ki samples are most different at 24 months of age, consistent with the basal deposit phenotype being most evident at this age. (**B**) HCA was performed as described, using the K-nearest-neighbor method with 1 PC and normalized mean-centered data. These analyses showed the same relationships between samples as that observed in the PCA studies. That is, the 24-month-old ki and wt samples are most different from each other, with the ki BrCH data being most similar to the 24-month-old ki BrM data. (wt is wild type, ki is *Efemp1*$^{R345W/R345W}$ knock-in, B is Bruch's membrane, BrCh is Bruch's membrane/choroid, numbers indicate the age of the mice in months.)

approach is dependent on the differences in the normalized spectral counts between mutant and wt samples for each protein, not on the fold changes. Those protein changes that were >3 SD from the mean of the differences were considered significant.

The SD calculated for the 8 months data was used to define the random differences of those proteins unaffected by the genetic changes. These random differences include natural biological, sample preparation and instrumental factors. This was based on the following observations. The PCA score plot (Fig. 2A) showed strong similarity between the data for the wt and mutant samples at 8 months. The Pearson correlation coefficient between proteins from wt and mutant mice was 0.984 indicating a strong correlation. The slope for the plot of the normalized spectral counts for the proteins in wt versus the mutant mice was 0.975 ± 0.026 (data not shown). These three results suggest that the levels of the majority of the proteins were highly correlated and were unaffected at 8 months by the p.Arg345Trp mutation in *Efemp1*. In fact, only 21 of the 832 proteins analyzed in the 8 months data set were outside 3 SD.

Based on the SD of protein variation established using the 8 months data (SD = 0.298), the proteins exceeding the 3 SD limit for the other data sets were identified and their deviation was assumed to arise from the mutation. The numbers of proteins >3 SD at 14 and 24 months were 66 and 88, respectively, for BCh and 65 for 24 months BrM. The proteins for 24 months, BrCh and BrM, are listed in Tables 4 and 5, respectively.

The matched pair difference approach is biased toward high-abundance proteins. In contrast, the use of ratios or fold changes is biased toward low abundance proteins. Thus, high-abundance proteins with large changes in their normalized spectral counts may be considered significant even though the fold change is not large. Likewise, changes in low abundance proteins may not be considered significant when they may, in fact, be biologically significant. More emphasis was placed on the ratios of normalized spectral counts between the wt and mutant mice for the low abundance proteins. Examples for low abundance proteins with significantly altered ratios in the mutant mice include collagen IV, alpha 1 which was decreased 10-fold and tenascin C and complement C4 which were increased 4.9- and 4.3-fold, respectively.

Biological processes of significantly altered proteins in mutant mice

Each protein in Tables 2–5 was annotated according to its associated biological processes using the Panther Classification system (86) and Mouse Genome Informatics (87). Immune system processes, cell–cell and cell–matrix adhesion, signal transduction and intracellular protein transport contributed the most to the differences observed in the mutant mice. Other biological processes such as proteolysis, apoptosis, lipid-related processes, cellular morphogenesis and angiogenesis were represented but to a much lesser extent. The number of proteins that contributed to each of these four major biological processes and the gene symbol for all of the proteins included for each biological process are summarized in Figure 3. The majority of proteins identified by the matched pair analysis overlap with those identified as major contributors in the PCA. As examples of proteins in these four categories, the following changes were observed.

Immune system processes

Immune system processes include complement activation, macrophage activation, B-cell-mediated immunity and antigen presentation and processing. Over 150 proteins with roles in these processes were identified in the eight data sets. Of these, 43 proteins were significantly altered in 24 months mutant mice or contributed significantly to PC1 and PC2 (Fig. 3). A few of these proteins changed progressively with age from 8 to 24 months. Thrombospondin 1 increased 13-fold in the mutant mice. Leukotriene A4 hydrolase was 8-fold higher in the mutant mice as a result of a comparable decrease with age in the wt mice. Macrophage migration inhibitory factor also decreased nearly 10-fold in the wt mice from 8 to 24 months.

Table 2. Proteins that contribute most significantly to PC1

Loadings[a]	Proteins 1–30	Gene	Loadings[a]	Proteins 31–60	Gene
0.169	Milk fat globule-EGF factor 8 protein	*Mfge8*	0.075	Macrophage migration inhibitory factor	*Mif*
0.144	Trifunctional protein, alpha subunit	*Hadha*	0.073	Perlecan (heparan sulfate proteoglycan 2)	*Hspg2*
0.138	Trypsin 10	*Try10*	0.073	Synaptophysin-like protein	*Sypl1*
0.138	Thrombospondin 1	*Thbs1*	0.072	Cell adhesion molecule 1/nectin-like 2	*Cadm1*
0.129	Galectin-3	*Lgals3*	0.069	Immunoglobulin heavy chain complex	*Igh*
0.128	Cathepsin B	*Ctsb*	0.068	Fibrinogen alpha chain	*Fga*
0.120	Collagen, type VI, alpha 3	*Col6a3*	0.068	Methyltransferase like 7A1	*Mettl7a1*
0.118	Cytochrome *c* oxidase subunit I	*mt-Co1*	0.067	Decorin	*Dcn*
0.115	Efemp1	*Efemp1*	0.067	EH-domain containing 3	*Ehd3*
0.112	Biglycan precursor	*Bgn*	0.067	Ras homolog gene family, member C	*Rhoc*
0.110	Actin, beta-like 2	*Actbl2*	0.067	RAB5A, member RAS oncogene family	*Rab5a*
0.106	Tubulin beta-2A chain	*Tubb2a*	0.066	Fibrinogen gamma chain	*Fgg*
0.103	Lysozyme 2/lysozyme C-2 precursor	*Lyz2*	0.066	Glycoprotein (transmembrane) nmb	*Gpnmb*
0.101	Protease, serine, 1 (trypsin 1)	*Prss1*	0.066	Aquaporin-1	*Aqp1*
0.099	Interferon-induced transmembrane protein 3	*Ifitm3*	0.066	PRA1 family protein 2	*Praf2*
0.098	Collagen, type VI, alpha 1	*Col6a1*	0.065	Tubulin, alpha 1A	*Tuba1a*
0.097	Olfactory receptor 485	*Olfr485*	0.065	Actin, beta	*Actb*
0.096	Sec61 alpha 1 subunit (*S. cerevisiae*)	*Sec61a1*	0.065	Translocase, outer mitochondrial membrane 40 homolog (yeast)	*Tomm40*
0.096	ATPase, H+ transporting, lysosomal V0 subunit C	*Atp6v0c*	0.065	Myosin, light chain 12B, regulatory	*Myl12b*
0.088	Histidine triad nucleotide-binding protein 1	*Hint1*	0.064	ATPase, H+ transporting, lysosomal V0 subunit D2	*Atp6v0d2*
0.085	Syndecan-binding protein	*Sdcbp*	0.063	Calsequestrin-1 precursor	*Casq1*
0.083	Collagen, type VI, alpha 2	*Col6a2*	0.063	Ig mu chain C region secreted form	*Igh-6*
0.082	Heat-shock protein 2	*Hspa2*	0.063	ADAMTS-like protein 5 isoform 1 precursor	*Adamts5*
0.081	6-Phosphogluconolactonase	*Pgls*	0.063	Phosphatidic acid phosphatase type 2A	*Ppap2a*
0.079	Podocalyxin-like	*Podxl*	0.062	Immunity-related GTPase family M member 1	*Irgm1*
0.078	Lumican	*Lum*	0.061	Translocase of outer mitochondrial membrane 22 homolog (yeast)	*Tomm22*
0.078	CD63 antigen	*Cd63*	0.061	Histocompatibility 2, K1, K region	*H2-K1*
0.077	Tyrosinase-related protein 1	*Tyrp1*	0.061	NADH dehydrogenase (ubiquinone) 1 alpha subcomplex, 5	*Ndufa5*
0.076	Complement factor H-related 2	*Cfhr2*	0.061	RAB32, member RAS oncogene family	*Rab32*
0.075	Actin, alpha, cardiac muscle 1	*Actc1*	0.061	Olfactory receptor 810	*Olfr810*

[a]Absolute loadings. Loadings indicate the contribution of each protein to PC1.

Eleven of the major components of the three complement pathways were identified in the eight data sets although, as expected, the abundance of each was low (Table 6). C3 was increased (1.8-fold) in the *Efemp1*$^{R345W/R345W}$ mice in 24 months BrM and was increased at younger ages in BrCh in the *Efemp1*$^{R345W/R345W}$ mice. CFH was present at comparable levels in the 24 months mice, wt and mutant. Complement C1q (C1q) and mannose-binding lectin (MBL) which are recognition molecules for the classical and lectin pathways, respectively, were both identified and were present at low but comparable levels.

Of particular interest was the contribution of C4 to immune processes and signal transduction for PC2 (Fig. 3B). C4, a relatively low abundance protein, was increased >4-fold in the BrCH of mutant mice at 24 months and was present at the same increased level in BrM in the mutant mice. An increase in C4 in the mutant relative to the wt mice was apparent by 14 months in BrCh.

The peptides identified in complements C3 and C4 in 24 months BrM are in Supplementary Material, Table S3 and their locations in the proteins are illustrated in Figure 4. In C3, the majority of the peptides (11 of 15) detected in the wt and mutant mice were from the fragment C3dg. The C4 peptides detected were only present in the mutant mice and were located within the fragment C4d.

The locations of complements C3 and C4, CFH, MBL and thrombospondin1 in BrM were validated using immunofluorescence (Fig. 5). In addition, the relative levels of staining were consistent with the results obtained by mass spectrometry (Table 6). Staining for C3 was more intense in the mutant mice than in wt mice as previously reported (56), staining was more intense for C4 in mutant mice, and staining was comparable for CFH in both wt and mutant mice. MBL was weakly detectable in both the wt and mutant mice but there were a few regions of intense staining in the mutant mice.

Adhesion and signal transduction

The numbers of proteins involved in cell–cell and cell–matrix adhesion and in signal transduction that contributed significantly to the basal deposit phenotype and the gene symbols for these proteins are shown in Figure 3. ECM and ECM-associated proteins comprise the majority of the proteins that are associated with adhesion and signaling among those proteins that contribute most significantly to PC1 and PC2 and for those proteins that undergo the largest changes in BrCh and BrM as a result of the mutation in *Efemp1*. Many of the same proteins contribute to both adhesion and signaling processes. EFEMP1, collagens type VI, alpha 3 and alpha 1, thrombospondin 1 and milk fat globule-EGF factor 8 are among the proteins in each category

Table 3. Proteins that contribute most significantly to PC2

Loadings[a]	Proteins 1–30	Gene	Loadings[a]	Proteins 31–60	Gene
0.186	Tubulin, beta 6 class V	*Tubb6*	0.069	ATP synthase, H+ transporting, mitoF0 complex, subunit F2	*Atp5j2*
0.159	Endonuclease domain containing 1	*Endod1*	0.069	Solute carrier family 9 (sodium/hydrogen exchanger), 3 reg 2	*Slc9a3r2*
0.131	Lysosomal protein NCU-G1 precursor	*NCU-G1*	0.069	EH-domain containing 3	*Ehd3*
0.128	Trypsin 10	*Try10*	0.068	Collagen, type VI, alpha 3	*Col6a3*
0.119	Surfeit gene 4	*Surf4*	0.067	Barrier-to-autointegration factor	*Banf1*
0.112	Acyl-coenzyme A dehydrogenase, long-chain	*Acadl*	0.067	Creatine kinase Muscle	*Ckm*
0.109	Keratin 5	*Krt5*	0.067	Clathrin, heavy polypeptide (Hc)	*Cltc*
0.108	NADH dehydrogenase subunit 1	*Mtnd1*	0.067	Laminin, alpha 5	*Lama5*
0.103	Cytochrome *c* oxidase subunit I	*Cox1*	0.067	Leukotriene A4 hydrolase	*Lta4h*
0.102	Milk fat globule-EGF factor 8 protein	*Mfge8*	0.066	Ras homolog gene family, member A	*Rhoa*
0.090	Microfibrillar-associated protein 4	*Mfap4*	0.064	Collagen, type VI, alpha 1	*Col6a1*
0.090	Protease, serine, 1 (trypsin 1)	*Prss1*	0.064	Progesterone receptor membrane component 1	*Pgrmc1*
0.086	Tryptase beta 2	*Tpsb2*	0.064	Lactate dehydrogenase B	*Ldhb*
0.085	Calmodulin 1	*Calm1*	0.064	Gelsolin	*Gsn*
0.082	Thrombospondin 1	*Thbs1*	0.063	ATPase, Ca^{2+} transporting, cardiac muscle, fast twitch 1	*Atp2a1*
0.082	Lysosomal-associated membrane protein 2	*Lamp2*	0.063	Capping protein (actin filament) muscle Z-line, alpha 2	*Capza2*
0.081	Lysosomal-associated membrane protein 1	*Lamp1*	0.062	Tubulin beta-2A chain	*Tubb2a*
0.081	Glutathione *S*-transferase, pi 1	*Gstp1*	0.062	Cysteine and glycine-rich protein 1	*Csrp1*
0.080	Eukaryotic translation elongation factor 1 alpha 1	*Eef1a1*	0.061	Fusion, derived from t(1216) malignant liposarcoma (human)	*Fus*
0.079	Myosin, light chain 12B, regulatory	*Myl12b*	0.061	Actin, beta	*Actb*
0.079	Reticulon 4	*Rtn4*	0.061	Profilin 1	*Pfn1*
0.078	Cytochrome *b*-5	*Cyb5a*	0.060	Guanine nucleotide-binding protein, alpha 11	*Gna11*
0.076	EH-domain containing 4	*Ehd4*	0.060	Malate dehydrogenase 1, NAD (soluble)	*Mdh1*
0.072	DnaJ (Hsp40) homolog, subfamily C, member 5	*Dnajc5*	0.060	Phospholipid scramblase 3	*Plscr3*
0.072	6-Phosphogluconolactonase	*Pgls*	0.060	Efemp1	*Efemp1*
0.070	Laminin, gamma 1	*Lamc1*	0.059	Aldo-keto reductase family 1, mem A1 (aldehyde reductase)	*Akr1a4*
0.070	Ezrin	*Ezr*	0.059	Chymase 1, mast cell	*Cma1*
0.070	Annexin A3	*Anxa3*	0.059	Collagen, type I, alpha 1	*Col1a1*
0.069	Heat-shock protein 90 alpha (cytosolic), class B member 1	*Hsp90ab1*	0.059	RAS-related protein-1a	*Rap1a*
0.069	Tubulin, alpha 1A	*Tuba1a*	0.059	Glyceraldehyde-3-phosphate dehydrogenase-like isoform 2	*Gapdh*
0.069	Methyl CpG-binding protein 2	*Mecp2*	0.055	Complement component 4B	*C4b*

for both adhesion and signaling processes. Each of these was increased. The relative increase of thrombospondin 1 in mutant mice is evident in Figure 5. The matricellular proteins, decorin and biglycan, which have roles in both adhesion and signaling were increased. The laminins were decreased. Perlecan which contributed most significantly to adhesion and signaling only in PC1 (age) was notable in that it decreased progressively with age in the wt mice and decreased further in the mutant mice to 20% of the level at 8 months (Supplementary Material, Table S1).

Intracellular protein transport

Proteins annotated as having roles in intracellular protein transport include proteins known to be associated with lysosomes, with endocytic and exocytic processes, and in vesicle-mediated transport. The numbers of proteins involved in intracellular protein transport contributed almost equally to PC1 and PC2 and to the 24 months BrCH and BrM samples. However, only 7 of the proteins are the same for both PC1 and PC2, but 12 proteins are the same for BrM and BrCh (Fig. 3). Laminins (alpha 5 and beta 2), associated with endocytic processes, were two of only five ECM proteins associated with intracellular protein transport and both were decreased at 24 months. EH-domain containing protein 4, involved with regulation of early endosomal transport, and clathrin, which functions in receptor-mediated transport, contributed to PC1, BrM and BrCh but not PC2. Both were increased (88,89).

Role of complement in basal deposit formation

We chose to test the functional significance of our data analyses by focusing on the relevance of the complement system to a major histopathologic feature of the *Efemp1*$^{R345W/R345W}$ mice, i.e. the age-dependent formation of basal laminar deposits. This choice was based on the following: (1) the increased levels of C3 and C4 in BrM in the *Efemp1*$^{R345W/R345W}$ mice implicated the complement system in the formation of the basal laminar deposits; (2) the accumulation of an activation fragment of C4 in BrM, suggesting that complement activation had occurred in the mutant mice; and (3) the role of complement in human AMD.

Homozygous *Efemp1*$^{R345W/R345W}$:*C3*$^{-/-}$ double-mutant mice were generated to test the role of the complement system in basal laminar deposit formation. The rationale for using complement *C3*$^{-/-}$ mice was that the three complement pathways converge

Table 4. BrCh proteins: standard deviations (absolute) for differences between wt and *Efemp1*$^{R345W/R345W}$ mice

Proteins 1–35	Gene	SD	Proteins 36–69	Gene	SD
Tubulin, beta 6 class V	*Tubb6*	24.3	Eukaryotic translation elongation factor 1 alpha 1	*Eef1a1*	4.8
Glyceraldehyde-3-phosphate dehydrogenase	*Gapdh*	23.0	Efemp1	*Efemp1*	4.8
Actin, alpha cardiac muscle 1	*Actc1*	16.8	Glutathione *S*-transferase, pi 1	*Gstp1*	4.6
Biglycan	*Bgn*	14.1	Protease, serine, 1 (trypsin 1)	*Prss1*	4.6
Tubulin, alpha 1A	*Tuba1a*	11.7	Aldo-keto reductase family 1, member A1	*Akr1a4*	4.5
Collagen, type VI, alpha 1	*Col6a1*	11.0	Phosphoglycerate mutase 1	*Pgam1*	4.5
Milk fat globule-EGF factor 8 protein	*Mfge8*	9.9	Heat-shock protein 90 alpha (cytosolic)	*Hsp90ab1*	4.3
sec61 alpha 1 subunit (*S. cerevisiae*)	*Sec61a1*	9.2	Receptor accessory protein 5	*Reep5*	4.3
Monoglyceride lipase	*Mgll*	8.9	Cathepsin L	*Ctsl1*	4.2
CD63 antigen	*Cd63*	8.4	Myosin, light chain 12B, regulatory	*Myl12b*	4.2
Galectin-3	*Lgals3*	8.1	Myosin, light polypeptide 9, regulatory	*Myl9*	4.2
Collagen, type VI, alpha 3	*Col6a3*	8.0	EH-domain containing 4	*Ehd4*	4.0
Glycoprotein (transmembrane) nmb	*Gpnmb*	7.9	Signal sequence receptor, delta	*Ssr4*	4.0
Surfeit gene 4	*Surf4*	7.7	Synaptogyrin 1	*Syngr1*	4.0
Tubulin beta-2A chain	*Tubb2a*	7.6	Ezrin	*Ezr*	3.9
Vesicle amine transport1 homolog (*T. californica*)	*Vat1*	7.6	Guanine nucleotide-binding protein (G protein), b1	*Gnb1*	3.9
Cathepsin b	*Ctsb*	7.4	Perlecan (heparan sulfate proteoglycan 2)	*Hspg2*	3.9
Olfactory receptor 485	*Olfr485*	7.4	Fibrillin 1	*Fbn1*	3.5
Actin, cytoplasmic 1	*Actb*	7.1	Guanine nucleotide-binding protein (G protein), b2	*Gnb2l1*	3.5
Thrombospondin-1	*Thbs1*	7.0	Leukotriene A4 hydrolase	*Lta4h*	3.5
Vimentin	*Vim*	7.0	ADP-ribosylation factor-like protein 8B	*Arl8b*	3.4
Clathrin, heavy polypeptide (Hc)	*Cltc*	6.3	Cytochrome *b*-5	*Cyb5a*	3.4
Actin-related protein 2/3 complex, subunit 5-like	*Arpc5l*	5.9	PREDICTED high-mobility group protein B1-like	*Hmgb1*	3.4
Collagen, type VI, alpha 2	*Col6a2*	5.9	Integrin beta 4	*Itgb4*	3.4
Laminin, gamma 1	*Lamc1*	5.9	Lumican	*Lum*	3.4
Pyridoxal (pyridoxine, vitamin B6) kinase	*Pdxk*	5.9	Peptidyl-prolyl cis-trans isomerase A	*Ppia*	3.4
Myosin regulatory light chain 2-A (*R. norvegicus*)	*Rlc-a*	5.9	Novel protein similar splicing factor, arg/ser-rich 3	*Sfrs3*	3.4
Syndecan-binding protein	*Sdcbp*	5.8	Transketolase	*Tkt*	3.4
Histocompatibility 2, D region locus 1	*H2-D1*	5.7	Tryptase beta 2	*Tpsb2*	3.4
6-Phosphogluconolactonase	*Pgls*	5.6	Vesicle-associated membrane protein 2	*Vamp2*	3.4
Ubiquitin C	*Ubc*	5.4	Heat-shock protein 90, beta (Grp94), member 1	*Hsp90b1*	3.3
Decorin	*Dcn*	5.2	Laminin, alpha 5	*Lama5*	3.3
Tubulointerstitial nephritis antigen-like 1	*Tinagl1*	5.2	RAB1B, member RAS oncogene family	*Rab1b*	3.1
Moesin	*Msn*	4.9	Clusterin	*Clu*	3.0
ADP-ribosylation factor 3	*Arf3*	4.8			

The 19 mitochondria proteins with SD >3 were not included in this list. They did not contribute to the four biological processes.

at the point of complement C3. Thus, in the absence of an active complement C3, the complement system could not be activated. The mice were assessed at 14 months for basal laminar deposits using transmission electron microscopy. In the *Efemp1*$^{R345W/R345W}$ mice (Fig. 6A, panels A and B), contiguous basal laminar deposits were present. In addition, vacuoles are noted in the RPE and basal infoldings were not present. In contrast, basal deposits were absent in the homozygous *Efemp1*$^{R345W/R345W}$:*C3*$^{-/-}$ double-mutant mice (Fig. 6, panel C). Some vacuoles can be seen in the double-mutant mice but basal infoldings were preserved and the RPE cells had a more normal appearance.

A quantitative comparison of the mean areas of the deposits for the different mouse strains was performed as described in Materials and Methods. The total area of basal deposits in each image was determined for each mouse (average of 65 images per mouse) for each strain (Fig. 6). The means of the cumulative areas for each mouse strain were determined and are compared in Figure 6E. There was a significant decrease in the area of basal deposits in the *Efemp1*$^{R345W/R345W}$:*C3*$^{-/-}$ double-mutant mice. The differences between the means for the *Efemp1*$^{R345W/R345W}$ and the *Efemp1*$^{R345W/R345W}$:*C3*$^{-/-}$ mice were significant to >95% confidence interval (CI) and the differences between *Efemp1*$^{R345W/R345W}$ mice and control mice were significant at 94% CI. The difference between the means of the areas for the double-mutant mice and control mice (wt and *C3*$^{-/-}$) was not statistically significant. The area of deposits in one of the double-mutant mice was determined statistically to be an outlier but the data were still included in this analysis.

DISCUSSION

The results presented in this study provide insight into the role of complement in the early stages of macular degenerations and define the pathology in the BrM caused by the p.Arg345Trp mutation in *Efemp1*. A critical role for an active complement system in the formation of basal deposits was clearly demonstrated. Genetic disruption of complement *C3* inhibited the formation of basal deposits, preserved the basal infoldings and reduced the RPE pathology in the *Efemp1*$^{R345W/R345W}$ mice. As basal deposits are considered precursors to drusen the results of this study provide evidence of how complement may contribute to drusen formation. The mutation in *EFEMP1* causes the presence of extensive drusen in the inherited disorder, DHRD/ML, thus, a role for the complement system is implicated in the pathogenesis of DHRD/ML (60). Drusen are also a characteristic feature in

Table 5. Bruch's membrane proteins: SDs (absolute) for differences between wt and *Efemp1*$^{R345W/R345W}$-mutant mice

Proteins 1–33	Gene	SD	Proteins 34–65	Gene	SD
Actin, cytoplasmic 1	*Actb*	20.5	Spectrin alpha 2	*Sptan1*	4.7
Tubulin, beta 6 class V	*Tubb6*	19.1	Clathrin, heavy polypeptide (Hc)	*Cltc*	4.4
Endonuclease domain containing 1	*Endod1*	16.3	Collagen, type I, alpha 1	*Col1a1*	4.4
Milk fat globule-EGF factor 8 protein	*Mfge8*	13.9	EH-domain containing 4	*Ehd4*	4.4
Myosin, light chain 12B, regulatory	*Myl12b*	11.7	Ig mu chain C region secreted form	*Igh-6*	4.4
Efemp1	*Efemp1*	10.7	Podocalyxin-like	*Podxl*	4.1
Thrombospondin-1	*Thbs1*	9.9	ADP-ribosylation factor-like protein 8A	*Arl8a*	4.0
Collagen type VI, alpha 3	*Col6a3*	9.5	Lumican	*Lum*	4.0
Tubulin, alpha 1A	*Tuba1a*	9.3	Moesin	*Msn*	4.0
Laminin, gamma 1	*Lamc1*	9.0	Nidogen 2	*Nid2*	4.0
Actin, alpha cardiac muscle 1	*Actc1*	8.9	Myosin, light polypeptide 9, regulatory	*Myl9*	3.8
Collagen type VI, alpha 1	*Col6a1*	8.2	Decorin	*Dcn*	3.7
Vimentin	*Vim*	8.2	Galectin-3	*Lgals3*	3.7
Biglycan	*Bgn*	8.0	Nidogen 1	*Nid1*	3.7
Syndecan-binding protein	*Sdcbp*	7.7	Monoglyceride lipase	*Mgll*	3.6
Laminin, alpha 5	*Lama5*	7.6	Aldo-keto reductase family 1, A1	*Akr1a4*	3.4
Lysosomal-associated membrane protein 2	*Lamp1*	7.2	Aquaporin 1	*Aqp1*	3.4
Lysosomal protein NCU-G1 precursor	*NCU-G1*	6.7	Macrophage migration inhibitory factor	*Mif*	3.4
Glutathione *S*-transferase, pi 1	*Gstp1*	6.7	Surfeit gene 4	*Surf4*	3.4
Reticulon 4	*Rtn4*	6.7	Thymus cell antigen 1, theta	*Thy1*	3.4
Hydroxysteroid (17-beta) dehydrogenase 11	*Hsd17b11*	6.3	Fibrillin 1	*Fbn1*	3.1
DnaJ (Hsp40) homolog, subfamily C, 5	*Dnajc5*	6.2	Gelsolin	*Gsn*	3.1
6-Phosphogluconolactonase	*Pgls*	6.0	Cysteine and glycine-rich protein 1	*Csrp1*	3.0
Perlecan (heparan sulfate proteoglycan 2)	*Hspg2*	5.9	Ezrin	*Ezr*	3.0
Cathepsin D	*Ctsd*	5.8	Vitronectin	*Vtn*	3.0
Polymerase I and transcript release factor	*Ptrf*	5.8	ATP synthase, H+ transporting F1 complex, b	*Atp5b*	7.0
Eukaryotic translation elongation factor 1, a1	*Eef1a1*	5.4	Cytochrome *c* oxidase subunit I	*Cox1*	6.7
Glyceraldehyde-3-phosphate dehydrogenase	*Gapdh*	5.0	Cytochrome *c* oxidase subunit 5A	*Cox5a*	6.0
Interferon-induced transmembrane protein 3	*Ifitm3*	5.0	ATP synthase, H+ transporting F0 complex, d	*Atp5h*	4.4
Sec61 alpha 1 subunit (*S. cerevisiae*)	*Sec61a1*	5.0	Acyl-coenzyme A dehydrogenase, long-chain	*Acadl*	3.9
Spectrin beta 2	*Sptbn1*	5.0	Lactate dehydrogenase B	*Ldha*	3.2
Laminin, beta 2	*Lamb2*	4.9	Aldehyde dehydrogenase 2, mitochondrial	*Aldh2*	3.2
N-myc downstream regulated gene 1	*Ndrg1*	4.9			

AMD, suggesting that the results are relevant to that disorder as well.

Proteomics

A major goal of this study was to determine the mechanisms involved in basal deposit formation by identifying those proteins that were altered in response to the mutation in *Efemp1*. The proteomic experiments were optimized to solubilize and identify as many of the proteins as possible in the BrCh and BrM samples including the ECM proteins. The ECM and ECM-associated proteins comprise ∼10% of the proteins identified in BrM but ∼20% of the mass of the proteins. The remaining proteins, most of which are present in low abundance, were identified because of the high-sensitivity and high duty cycle of the UPLC and the mass spectrometer system used for the experiments. While the majority of the proteins detected in the BrM samples are thought to be from BrM itself, some proteins detected may be from the choriocapillaris which forms one layer of the BrM or from membrane fragments and cell debris trapped in basal deposits within a compromised BrM.

Biologically significant changes

Defining the biologically significant changes that were the result of the mutation in *Efemp1* presented a challenge. Since one focus of the study was on BrM, an ECM, labeling techniques were not considered feasible. Spectral counting is a successful method for quantifying proteins and normalized spectral counts have been successfully used to quantify cilia proteins and were used in this study (75,76,90). Replicates were not done at any one age; instead, data were collected at three ages and a comparison between BrCh and BrM was done at one age as this approach was the most efficient use of mass spectrometer instrument time, considering that multiple fractions per sample were analyzed to maximize depth of analysis.

We chose to use PCA to identify trends and those proteins that contribute to those trends (80). In addition, we chose to use the matched pair difference approach and the SD of differences to further analyze and understand the biological significance in the data (85). When the matched pair difference approach was applied to wt aging data, i.e. differences between 8 and 24 months, those proteins outside 3 SD were many of the same proteins that contributed to PC1 (age) (data not shown). This provided further confidence in the validity of the approaches used.

Some proteins were only identified in either wt or mutant samples at a given age and could reflect a technical issue rather than a biological difference between the mutant and wt samples. The matched pair difference approach provided a means of identifying whether any of those differences were significant. As indicated in the results, the matched pair difference approach is biased toward high-abundance proteins and the use of ratios is biased toward low abundance proteins. More emphasis was placed on the ratios of normalized spectral

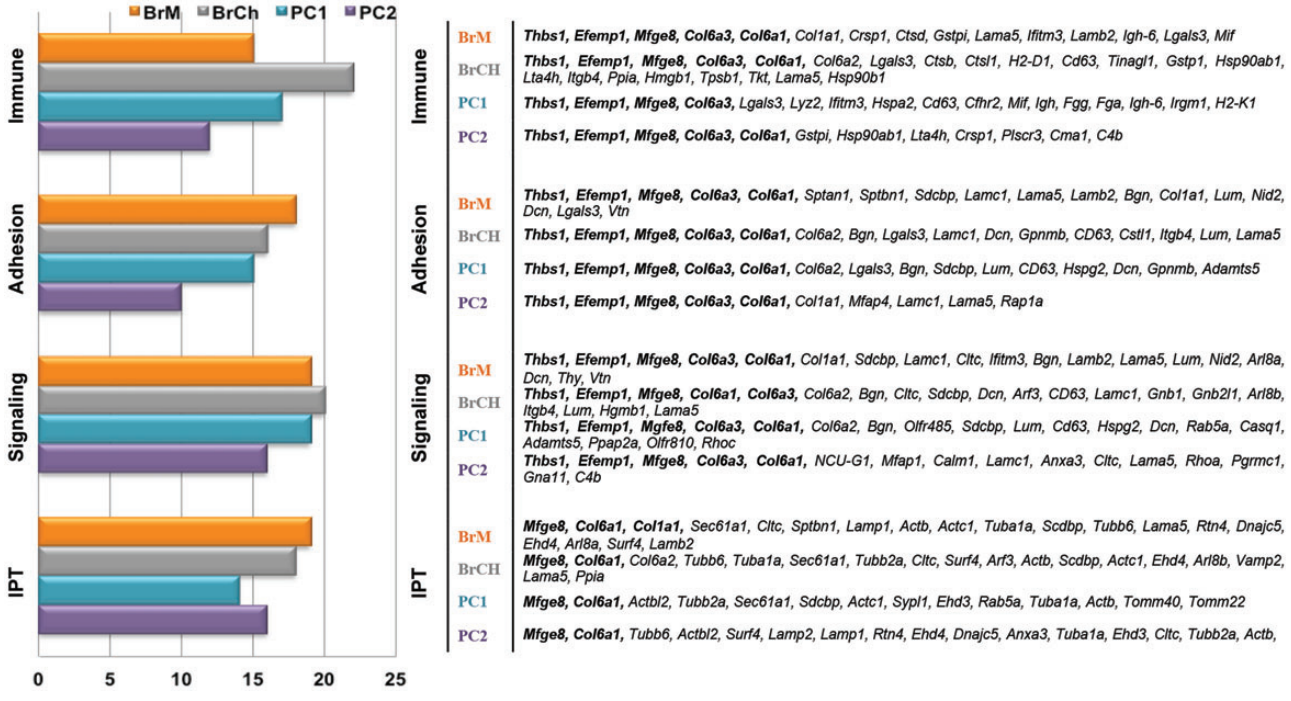

Figure 3. Left: major biological processes affected by the p.Arg345Trp mutation in *Efemp1*. The *x*-axis is the number of proteins that are changed by more than 3 SD in mutant mice (BrCh and BrM) and in the top 60 proteins contributing to PC1 (age) and PC2 (genetics). Immune: immune system processes including complement activation, macrophage activation, B-cell-mediated immunity, and antigen presentation and processing; adhesion: cell–cell and cell–matrix adhesion processes; signaling: signal transduction processes; IPT: intracellular protein transport including lysosomal, endocytic and exocytic processes, and vesicle-mediated transport. Right: gene symbols for those proteins annotated to each biological process.

Table 6. Complement components identified

Protein name	Gene	Spectral counts								Complement pathway
		8K	8W	14K	14W	24K	24W	24BK	24BW	
Complement C3	*C3*	59	47	78	57	39	39	61	33	Complement system
Complement C4B	*C4B*	14		70	20	39	9	39		Classical, lectin
Complement C5	*C5*					2		3		Complement system
Complement C9	*C9*							3		Complement system
Complement factor H	*Cfh*	23	11	19	13	19	26	36	35	Alternative, regulatory
Complement Cfh-related 2	*Cfhr2*			21	17	18	31	27	32	Alternative, regulatory
Complement component 1 Q subcomponent-bp	*C1qbp*	4	10	2	5	6	6	2	4	Classical, inhibits C1
Complement C1q subunit A	*C1qa*	3	2	5	2	4				Classical
Complement C1q subcomponent subunit B	*C1qb*	2	3			4	2	4		Classical
Complement C1q subunit C	*C1qc*	4				3				Classical
Lectin, mannose-binding 2	*Lman2*	9	6			5	6	7	3	Lectin

counts between the wt and mutant for the low abundance proteins. Two such significant examples for low abundance proteins with increased ratios in the mutant mice were complement C4 and C3. The significance of the changes in C3 and C4 based in this case on ratios was evident from the demonstration that complement has a necessary role in basal deposit formation.

Complement

While it was clearly shown in this study that active complement C3 is necessary for basal deposit formation in the *Efemp1*$^{R345W/R345W}$ mice, the underlying mechanisms by which the complement system contributes to basal deposit formation remain to be identified. The complement pathway that initiates the involvement of the complement system in basal deposit formation in the *Efemp1*$^{R345W/R345W}$ mice is not known. There are three pathways by which the complement system is typically activated, the classical, lectin and alternative pathways (24,25,91,92). The classical pathway is typically activated by immune complexes, the lectin pathway is activated by surface patterns and the alternative pathway is constitutively active at a low level. All three pathways can be activated by altered patterns caused by foreign proteins or damaged self (93).

Genetic studies which showed that variants of complement factors H and B correlated with a risk of developing AMD focused attention on the importance of the alternative pathway (12–17,19,21). The alternative pathway has also been

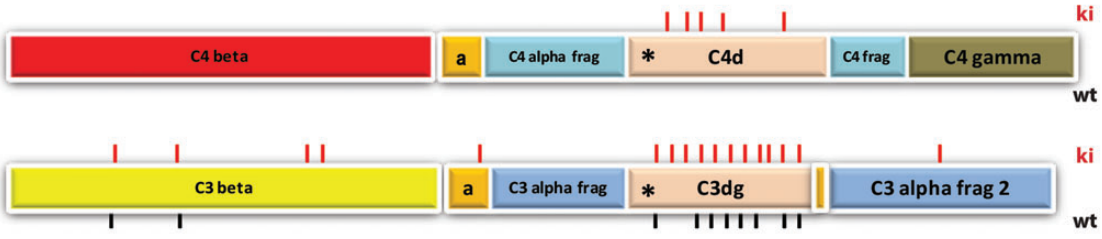

Figure 4. Depiction of activation fragments of C4 and C3 with the location of peptides identified by mass spectrometry indicated. Black lines: C3 peptides identified in wt mice. Red lines: C3 and C4 peptides identified in *Efemp1*$^{R345W/R345W}$ mutant mice. Asterisk indicates the location of the reactive thiol ester. The fragmentation pattern for C4 is modeled after human C4B.

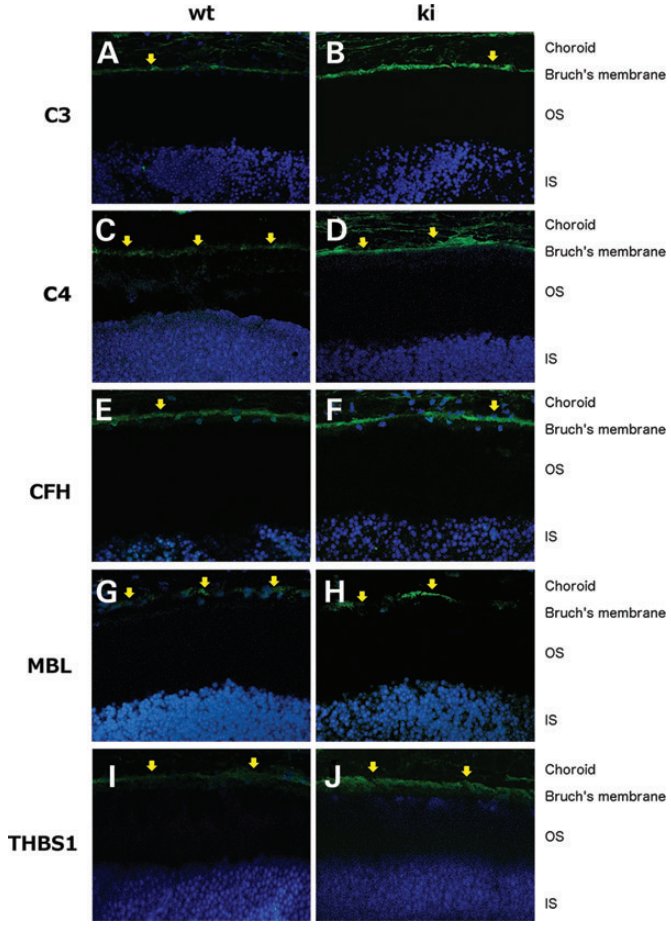

Figure 5. Confocal fluorescent images of cryosections stained with antibodies to the indicated proteins on the left of the figure. Sections were from 19-month-old mice. (wt is wild type, ki is *Efemp1*$^{R345W/R345W}$ knock-in mice.) Scale bar is 10 μm.

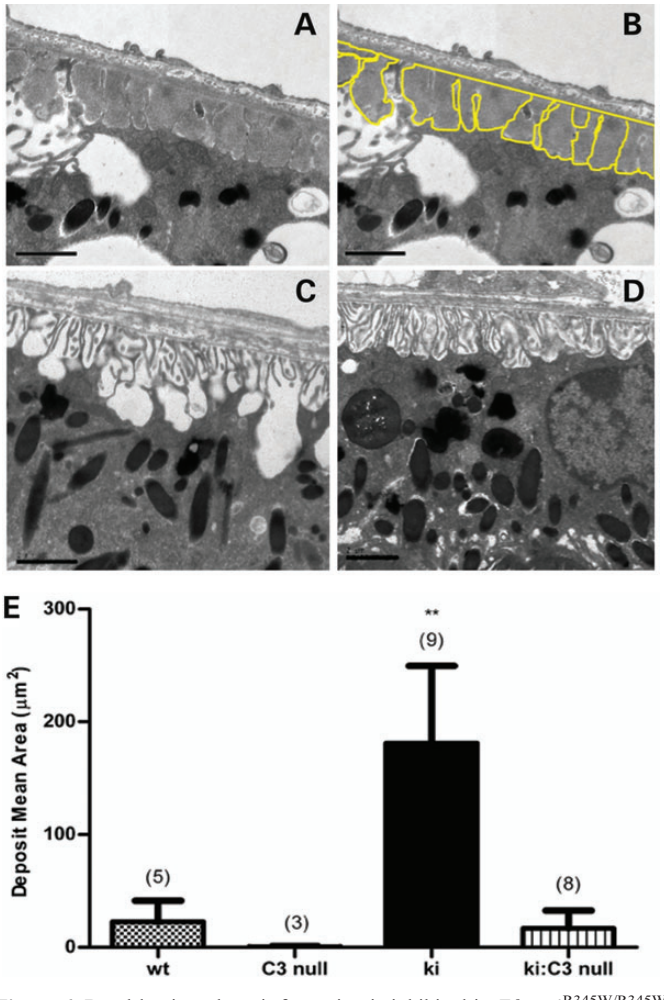

Figure 6. Basal laminar deposit formation is inhibited in *Efemp1*$^{R345W/R345W}$ mutant mice that are null for complement C3. Transmission electron micrographs are shown for 14 month old mice. (**A** and **B**) Basal laminar deposits are present in *Efemp1*$^{R345W/R345W}$-mutant mice between the RPE and BrM. The deposits are outlined in (B). (**C** and **D**) *Efemp1*$^{R345W/R345W}$:*C3*$^{-/-}$ double mutant mice (C) and wt mice of the same age (D) do not have basal deposits. (**E**) The mean area of basal deposits is plotted for each mouse strain: control mice (wt and *C3* null), small hatch bars; *Efemp1*$^{R345W/R345W}$ mutant mice (ki), black bar; and *Efemp1*$^{R345W/R345W}$:*C3*$^{-/-}$ double mutant mice (ki:C3 null), striped bar. The error bars are standard error of the mean. Double asterisks indicate the difference between the *Efemp1*$^{R345W/R345W}$ mice and *Efemp1*$^{R345W/R345W}$:C3$^{-/-}$ double mutant mice was significant (>95% CI). The difference between the *Efemp1*$^{R345W/R345W}$ and control mice was significant to 94% CI. The number of mice is indicated above the error bars. The mean area of deposits for the double mutant mice is markedly reduced relative to that for the *Efemp1*$^{R345W/R345W}$ mutant mice and is comparable to that for the wt mice.

considered key in other human diseases (24,25,94). We found no direct evidence to suggest the alternative pathway was or was not involved in basal deposit formation in the *Efemp1*$^{R345W/R345W}$ mice. Complement factor B was not detected and the levels of complement factor H were comparable in both the wt and mutant mice (Table 5 and Fig. 4). A role for either the classical or the lectin pathway in initiating the involvement of the complement system was suggested by two observations: (1) low levels of the recognition molecules for both the classical and lectin pathways, C1q and MBL, respectively, were present, and (2)

levels of C4 were increased in BrM in the mutant mice. C4 participates in the activation of both the classical and lectin pathways. Evidence obtained using a cell culture model of human RPE cells that mimics the formation of drusen, suggested activation in that system was initiated by the classical pathway through binding of C1q to lipid rich protein deposits (95).

We propose that the altered components of BrM in the mutant mice led to the involvement of immune processes and the activation of the complement system by exposing new surfaces or neo-epitopes that then interact with the recognition molecules of the appropriate complement pathway. Increased levels of C3 and C4 peptides were found in BrCh by 14 months, and were derived from the activation fragments of C3 and C4, C3dg and C4d, respectively, in 24 months BrM. C3dg and C4d contain the reactive thiol ester that can covalently attach C3 and C4 to target sites (96–99). This implies that BrM components in the *Efemp1*$^{R345W/R345W}$ mice are recognized by the complement system, and may indicate that this recognition plays a role in deposit formation by activating the complement system.

It is known that alterations in the integrity of ECM and variants in components of ECM contribute to the pathogenesis of AMD (49,100,101). Further, mutations in *EFEMP1*, *TIMP3* and *CTRP5*, all of which encode ECM proteins, lead to inherited macular degenerations (56,63,74,102). Models of the inherited macular degenerations caused by mutations in each of these genes develop basal deposits, suggesting that the underlying mechanisms may be similar and may involve complement (54–56,59,103).

Altered biological processes

The assignment of biological processes to those proteins that undergo large changes as a result of the mutation provides some assessment of what functions may be impacted by the p.Arg345Trp mutation in *Efemp1*. However, each protein may be assigned to more than one biological process and the major biological role of that protein may not be discernible from the assignments. Regardless, it provides direction and the basis of future investigations into how the *Efemp1*$^{R345W/R345W}$ mutation affects the function of the RPE/BrM/Choroid complex and leads to basal deposit formation. The largest impact appeared to be on immune system processes, cell–cell and cell–matrix adhesion, signal transduction and intracellular protein transport (Fig. 3). The role of the immune system in drusen formation was implicated previously (27). The results of this study support and extend the role of the immune system, in particular, the complement system in drusen formation.

Changes in the level of proteins with roles in intracellular protein transport are evidence that exo- and endocytic processes, vesicle transport and possibly lysosomal function are impacted by the mutation in *Efemp1*. This is consistent with the presence of vacuoles in the RPE as early as 2 months in the mutant mice and their enlargement with increasing age (56).

ECM and ECM-associated proteins are prominently represented in each of these biological processes and are prominent among the proteins with the major changes induced by the mutation in *Efemp1*. As would be expected for an ECM, the altered levels of ECM proteins lead to disruption of cell–cell and cell–matrix adhesion and the inherent signaling processes that rely on the structural integrity of the ECM (77). How these changes specifically lead to basal deposit formation is not clear. Four ECM and ECM-associated proteins stand out as being particularly significant in the mutant based on their large increase in the BrM of mutant mice. These are EFEMP1, thrombospondin 1, milk fat globule-EGF factor 8 and collagen VI. As described briefly below, each is involved in multiple cellular processes and/or the structure and function of the ECM.

EFEMP1

The phenotypic effects of the Arg345Trp mutation in EFEMP1 can be seen by 2 months when vacuoles are present in the RPE and wide-spaced collagen is present in BrM. Basal deposits become visible shortly thereafter. Yet the number of proteins increased or decreased in mutant BrCh is small even at 8 months. The major protein changes are not seen in the mutant mice until after 14 months with large changes observed in BrM proteins at 24 months. EFEMP1 accumulates in BrM of mutant mice. The accumulation in BrM could be due to increased expression and secretion or decreased turnover. Decreased secretion of the protein from cells in culture was reported but EFEMP1 appears to be efficiently secreted in the mutant mice (57,104,105). The Arg345Trp mutation in EFEMP1, which leads to increased levels of EFEMP1, may also lead to an altered conformation of the protein or altered interactions with components of BrM, any of which may cause the disrupted structure of BrM.

EFEMP1 is a binding partner to TIMP3 which is an inhibitor of matrix metallo-proteinases, but it is not known whether the Arg345Trp mutation influences the interaction with TIMP3 and the turnover of matrix components including EFEMP1 (73). EFEMP1 has function in the integrity of elastic fiber integrity in some tissues, and is also important in tumor growth where it activates signaling pathways through an interaction with EGF receptors and may alter cell motility (67,69–72). The specific mechanisms by which the Arg345Trp mutation in EFEMP1 leads to the pathology are under investigation.

Thrombospondin 1

The increase in thrombospondin 1 is the largest observed for any protein in the *Efemp1*$^{R345W/R345W}$ mice. Thrombospondin 1, a multi-domain protein, activates TGFbeta, initiates signal transduction, functions in the immune system and is involved in inflammation and wound healing (106–108). It is secreted by the RPE, is a component of BrM, choriocapillaris and larger vessels, and is important for retinal and choroidal vascular homeostasis (109–112). Thrombospondin 1 modulates angiogenesis (106–108). Mimetics of the type 1 repeats and the procollagen domains are anti-angiogenic and are being used to treat neovascular disease (113). A role of thrombospondin 1 in AMD is suggested by its presence in drusen (114). What function the increase in the *Efemp1*$^{R345W/R345W}$ mice may have and what stimulates its increase are not known but these questions warrant further study.

Milk fat globule-EGF factor 8 protein

Milk fat globule-EGF factor 8 protein (MFGE8), also known as lactadherin, is a pleiotropic, secreted glycoprotein that is a

component of BrM. The contribution of MFGE8 to PC1 and PC2 was highly significant and the protein was one of the most increased in the mutant mice. Its role in BrM in the mutant mice is totally unknown but a few of its reported functions may be significant in the mutant mice. MFGE8 is a ligand for alphavbeta5 integrin and is involved in the phagocytosis of photoreceptor outer segment discs by the RPE (115). MFGE8 limits inflammation and promotes tissue homeostasis through its role in clearing apoptotic bodies by bridging apoptotic bodies and phagocytic cells. MFGE8 is also thought to negatively regulate fibrosis by facilitating the removal of accumulated collagen, a function which may be relevant to BrM (116).

Collagen VI

Collagen VI comprises three chains, alpha 1, alpha 2 and alpha 3, and ultimately forms tetramers. This protein is an important component of extracellular matrices and is found in most interstitial tissues (117). Biglycan and decorin, both of which were increased, bind collagen VI and are involved in fibril formation (118–120). Collagen VI is an abundant component of the BrM proteome as reported here and was observed in BrM by immunostaining (121). In the *Efemp1*$^{R345W/R345W}$ mice, collagen VI was the only collagen that was not decreased and was slightly increased. It will be important to our understanding of basal deposit formation to determine if collagen VI is a major component of deposits and, if it is, what leads to its altered structure and increased presence.

Basal deposits

New proteins in the BrM of *Efemp1*$^{R345W/R345W}$ mice that could explain the composition of the basal deposits were not identified in the proteomic analyses reported here. This led us to propose that the basal deposits comprise proteins normally present in BrM but with altered levels and/or structures. For example, as early as 2 months, wide-spaced collagen was observed in BrM of *Efemp1*$^{R345W/R345W}$ mice (56). Wide-spaced collagen is also visible in the basal laminar deposits associated with BrM in the lower right of Figure 1.

Wide-spaced collagen has been observed in other ocular tissues such as epiretinal membranes and tissue samples from patients with AMD and Sorsby's fundus dystrophy (52,122).

Several structural studies on the wide-spaced collagen in these tissues led to the conclusion that collagen VI is at least one component of these structures (52,122–124). Collagen type IV, laminin, and fibronectin have been described as components of basal laminar deposits (51). In the present study, collagen type IV and laminins were less abundant in the mutant mice than in wt mice, whereas collagen VI, an abundant protein in the BrM proteome, was increased in the mutant mice. While it is tempting to speculate that an altered structure of collagen VI may be a major component of basal laminar deposits and the wide-spaced collagen, additional evidence for this is needed.

The proteomic analyses identified structural proteins that are present in deposits such as collagens; however, we also think that a subset of proteins in the deposits may have a causative role in deposit formation. The detection of multiple complement system components in the deposits led us to the hypothesis that complement activation could be a causal factor in deposit formation. This hypothesis turned out to be true, and the results suggest an early role for perturbations to the complement system in deposit formation and macular degeneration pathogenesis. Studies of additional deposit components will be needed to identify other causative factors in deposit formation. It is also possible that factors which are not deposit components could play a role in initiating deposit formation, such as alterations in RPE function.

Comparison with human study

A proteomic study of human BrCh identified 901 proteins that were presence with varied frequency in 24 patients with AMD (125). A similar number of proteins (1062) were identified in this study in three ages of BrCh and 24 months BrM from wt and *Efemp1*$^{R345W/R345W}$ mice. About 50% of the proteins identified in the human BrCh were also identified in the mouse samples, which is excellent concordance for proteomics experiments using somewhat different methods (125). Most importantly, similar trends in the data between the two studies were observed. Seven of the 14 proteins that were less abundant in AMD were also decreased in the 24-month-old mutant mice. Nineteen of the 45 proteins that were more abundant in AMD were identified and 25% of those were increased in the mutant mice. Five proteins that were less abundant in early-to-mid AMD were also decreased in mutant mice. Four proteins that were increased in more advanced AMD, dry and neovascular, were likewise increased in the mutant mice. These were complement C3, vitronectin, galectin 3 and Ig mu chain C region, all of which have roles in the immune system. Complements C3 and C4 were elevated to a greater extent in the mutant mice than in the AMD samples. CFH was not increased in the mutant mice but CFH was slightly increased in the AMD samples. While there were quantitative differences in the results between these two studies, there was a remarkable concurrence of results between a mouse model of an inherited macular dystrophy and human BrCh in AMD. This concurrence provides validation for the use of the *Efemp1*$^{R345W/R345W}$ mouse model to study the pathogenesis of basal deposit formation in early macular degenerations.

MATERIALS AND METHODS

Mice

The use of the mice in this study was approved by the Massachusetts Eye and Ear Infirmary and Harvard Medical School Animal Care and Use Committees. The point mutation knock-in mice (*Efemp1*$^{R345W/R345W}$ mice) made in this laboratory were previously described (56). *C3* null mice (*C3*$^{-/-}$) had 105 bp of exon 1 and 2.3 kb of the 5′ flanking region disrupted with a neocassette transcriptionally opposite the C3 gene (126). Messenger RNA and protein were not expressed in the liver, there was no circulating C3, and the mice were functionally null for C3. A nonfunctional C3 protein expressed in other tissues is missing the leader sequence preventing native processing and secretion of the protein (126). C3 was not properly processed in our *C3* null mice; the 10K fragment was not generated as seen in *C3*$^{+/+}$ mice (Supplementary Material, Fig. S2).

Homozygous *Efemp1*$^{R345W/R345W}$:*C3*$^{-/-}$ double-mutant mice were generated by crosses of the two strains. The double-mutant mice were viable, grossly normal, and had a normal lifespan. Control *C3* null mice were obtained during the generation of the double-mutant mice and were subsequently bred. Littermate wt mice were used when possible but this was not always possible considering some of the mice were aged 24 months. In those cases, the wt mice were from the same colony but different breeders.

Genotyping

The primers used to genotype the mice are shown in Supplementary Material, Table S4. Genomic DNA was prepared from tail snips or ear clips using the DNeasy kit following the manufacturer's instructions (Qiagen, Valencia, CA, USA). TaqMan polymerase, dNTP mix and reaction buffer were from Roche Applied Science (Indianapolis, IN, USA) and primers were from Integrated DNA Technologies (Coralville, IA, USA). PCR reactions for *Efemp1* ki and wt and for *C3* null were performed using 50 ng genomic DNA in 25 μl containing 25 nmol primers. PCR for *C3* wt was done using 25 nmol primers in Green PCR Master Mix following the manufacturer's protocol (Fermentas Life Sciences, Lafayette, CO, USA). PCR conditions for *Efemp1* ki and wt were as follows: 94°C for 3 min and 35 cycles of 94°C for 30 s, 57°C for 30 s and 72°C for 1 min followed by 94°C for 5 min. PCR conditions for *C3* null and wt were as follows: 94°C for 3 min and 30 cycles of 94°C for 1 min, 60°C for 1 min and 72°C for 1 min followed by 72°C for 2 min. PCR products were electrophoresed in a 1.5% agarose gel and visualized by SYBR Safe DNA gel stain (Invitrogen, Life Technologies, Grand Island, NY, USA).

Electron microscopy

Fourteen-month-old mice were euthanized with CO_2 gas and perfused transcardially with 10 ml fresh 2% paraformaldehye/2% glutaraldehyde in 0.1 M phosphate buffer, pH 7.4. The eyes were removed and placed in the same fixative for 3 h on ice. Eye cups were prepared by cutting just below the ora serrata and removing the anterior segment. After washing twice for 5 min in 0.1 M phosphate buffer (pH 7.4), the retina was cut into vertical oriented sections that extended from the optic nerve to the periphery. These were left in phosphate buffer at 4°C for 3 h. Standard techniques were used to prepare the samples for electron microscopy. Briefly, the samples were post-fixed in 1% osmium tetroxide in 0.1 M phosphate buffer for 1 h. After washing, the samples were dehydrated in increasing concentrations of ethanol (50, 70, 80, 95 and 100%) and finally in propylene oxide. Samples were embedded using the medium formulation of Embed 812 (Electron Microscopy Sciences, Hatfield, PA, USA).

Transmission electron microscopy was performed on the Tecnai 12T transmission electron microscope and images were visualized using DigitalMicrograph (Gatan, Inc., Warrendale, PA, USA). To obtain a random, unbiased sampling of the retina in each mouse, electron microscope images were recorded every 25 μm from the optic nerve to the retinal periphery. The area of the basal deposits in each micrograph (65 micrographs per mouse) was determined using ImageJ software (127). The mean of the total areas for each mouse strain were compared among the four strains. A two way *t*-test was used to determine the statistical significance of the comparison of the means of deposit areas among the mouse strains.

Immunofluorescence

Mice were euthanized and perfused with PBS. The eyes were removed, washed with PBS and cleaned of tissue. The whole eyes were placed in OCT (Electron Microscopy Sciences, Hatfield, PA, USA) and quick frozen. Twelve-micron thick cryosections were cut, dried onto Colorfrost Plus slides and stored at −80°C until use.

Antibody reactivity

Anti-C3 (Ab11862), anti-C4 (Ab11863), anti-CFH (Ab53800), anti-MBL (Ab106046) and anti-thrombospondin (A6.1) were from Abcam Inc. (Cambridge, MA, USA). Cryosections were dried at room temperature for 1 h. The tissue samples were fixed with cold acetone for 10 min and were rehydrated with PBS for 10 min. Samples were blocked with 1% BSA in PBS for 1 h at room temperature. Primary and secondary antibodies were diluted in the sample buffer. Incubation with the primary antibody was performed at 4°C overnight in a humid chamber. Samples were washed three times for 10 min each with PBS. Incubation with secondary antibodies was done for 1 h at room temperature. Samples were again washed three times for 10 min each with PBS. Vectashield with DAPI (Vector Laboratories, Inc., Burlingame, CA, USA) was added and a coverslip was placed onto the slide.

Confocal microscopy

Confocal microscopy was performed using a Leica SP5 microscope and LASAF software (Leica Microsystems Inc., Buffalo Grove, IL, USA). All sections were analyzed at 7% laser power except when using antibodies to CFH when the laser power was 40%. The objective used was ×63 oil.

Sample preparation

For consistent sample preparation, all samples were dissected and prepared by the same person. BrCh, BrM and basal deposits (BrM with deposits) were prepared as follows. Eye cups were made and the neural retina was peeled out. The eye cups were filled with PBS (without Mg^{2+} and Ca^{2+}) and frozen at −80°C until used. Room temperature PBS was added to thaw the sample. Cuts were made to flatten the eye cup. The eye cup was vortexed briefly in PBS. Remaining RPE cells were removed by washing the BrM using a stream of PBS. The BrCh was manually peeled from the sclera. Basal deposits remained associated with the BrM (Fig. 1). BrM samples were prepared by dissecting out the BrM and manually removing the remaining choroid from the BrM. An electron micrograph of isolated BrM is in Supplementary Material, Figure S3. The proteins in the BrCh and BrM preparations were solubilized in 1% SDS/8 M urea/50 mM DTT/25 mM EDTA by short bursts of sonication at 4°C. Insoluble material was removed by centrifugation twice for 40 min at 14 000 *g*.

The solubilized proteins obtained in the cleared supernatants from the mutant and control tissue samples were electrophoresed 2 cm into 1 mm SDS–PAGE gels, 4–12% acrylamide. The amounts of protein loaded onto the gels for each sample were comparable as determined by scanning the lanes of colloidal Coomassie stained gels (Invitrogen, Carlsbad, CA, USA) (128). Each gel lane was cut into 1 mm slices and the proteins in each slice were digested in-gel with trypsin. Each slice was treated as an individual sample, destained, dried in a Speedvac, reduced using 100 μl 20 mM Tris (2-carboxyethyl) phosphine hydrochloride in 25 mM ammonium bicarbonate (pH 8.0) and alkylated using 100 μl of 40 mM iodoacetamide in 25 mM ammonium bicarbonate (pH 8.0). After thorough washing, gel pieces were dried, rehydrated with 20 μl of 0.02 mg/ml modified trypsin (Promega, Madison, WI, USA) in 40 mM ammonium bicarbonate, and incubated overnight with shaking at 37°C. The gel slices were extracted with 20 μl of 40 mM ammonium bicarbonate, supernatants were combined and digestion was stopped by adding 4 μl concentrated acetic acid.

Mass spectrometry

Tryptic digests were analyzed by injecting 8 μml onto a 15-cm nanocapillary reverse-phase column (New Objective PicoFrit 75 μm column) terminating in a nanospray 15 μm tip self-packed with Microm Magic C18 AQ 200A, 5 μm resin, which was directly coupled to a ThermoElectron Orbitrap XL or ThermoElectron FTICR mass spectrometer. Peptides were eluted at a flow rate of 300 nl/min using 0.1% formic acid in MilliQ water as solvent A and 0.1% formic acid in acetonitrile as solvent B and a gradient consisting of: 3–50% B over 65.5 min, 50–80% B over 5 min, and a 5 min hold at 80% B. Mass spectral (MS) and MS/MS data were acquired in data-dependent mode with full MS scans from $m/z = 300$ to 2000 at 60 000 resolution using a top six method with a minimum MS signal threshold of 1000.

A customized database was created using the UniRef mouse database (downloaded multiple times until December 2011) with common contaminants such as trypsin, keratins and other environmental proteins added. A reverse database was produced by inverting each protein sequence and these sequences were appended in front of the forward sequences. The database was indexed using partial trypsin specificity, variable methionine sulfoxide oxidation and static cysteine modification as carboxyaminomethyl cysteine. MS/MS data were searched against these databases using the SEQUEST search engine within ThermoFisher Bioworks (Version 3.3.1) with a precursor mass tolerance of 100 ppm and fragment ion tolerance of 1 amu. Results were further processed using DtaSelect (versions 1.3 and 2.0). With DtaSelect, data were filtered using 10 ppm, full tryptic specificity, $\Delta C_n \geq 0.05$, and grouped peptides into consensus proteins and compared spectral counts between sample and control.

The output from Sequest was further analyzed using Scaffold software (Proteome Software, Inc., Portland, OR, USA). Proteins were identified by two or more peptides. Probabilities of peptide and protein identifications were >95 and 99%, respectively. Estimates of protein levels (abundance) were made from unweighted spectral counts and normalized using the number of theoretical tryptic peptides between m/z range of 750 and 3000 (76). The nuclear proteins were not included in the PCA.

Data analysis

PCA was applied to normalized spectral counts using Solo (Eigenvector Research Inc., Wenatchee, WA, USA) (80). The analysis yielded both the score plot and the loadings. Loadings are the measure of the contribution of each variable (each protein) to each PC (81). The percent variance in the loadings was calculated by squaring the loadings, summing the results for the desired number of proteins (variables) and multiplying by 100. HCA was performed using Solo (Eigenvector Research Inc.). The analysis was done on normalized spectral counts using a standard clustering algorithm (K nearest neighbor) (84).

Standard deviation of differences for proteomic data was done as follows. The mean and SD were determined using the 8 months data as control data for the other data sets. The mean of the differences for each protein was determined for these data and the SD of the distance from the mean for each protein was determined. Those proteins with differences that were >3 SD from the mean were considered to be proteins that were affected by the mutation or were outliers. For 8 month mice only 28 proteins were outside 3 SD from the mean (>99% CI). These proteins were removed and the calculations were repeated. The mean was 0.068. The SD of 0.298 was used to determine those proteins in the 14- and 24-month data sets that were >3 SD.

ECM and ECM-associated proteins were identified from the matrisome database (http://web.mit.edu/hyneslab/matrisome/). The biological processes associated with proteins were identified using the Panther database (www.pantherdb.org) and the Mouse Genome Informatics (MGI) Web, The Jackson Laboratory, Bar Harbor,ME, USA, World Wide Web (www.informatics.jax.org).

SUPPLEMENTARY MATERIAL

Supplementary Material is available at *HMG* online.

ACKNOWLEDGEMENTS

We thank Joseph White for helpful discussions, Daniel Harnly for his technical assistance and the Wistar Institute Proteomics Core Facility for performing the proteomics analyses.

Conflict of Interest statement. J.D.L. is the inventor of patents and/or patent applications that describe the use of complement inhibitors for therapeutic purposes and is the founder of Amyndas Pharmaceuticals which is developing complement inhibitors for clinical applications.

FUNDING

This work was supported by the Ocular Genomics Institute, Department of Ophthalmology, Harvard Medical School, Boston, MA 02114; the Rosanne Silbermann Foundation; the National Cancer Institute (NCI Cancer Core Grant CA010815 to The Wistar Institute); the National Eye Institute (MEEI Core Grant P30 EY014104) and the National Institutes of Health (AI068730 and EY020633 to J.D.L.).

REFERENCES

1. Michaelides, M., Hunt, D.M. and Moore, A.T. (2003) The genetics of inherited macular dystrophies. *J. Med. Genet.*, **40**, 641–650.
2. Klein, R., Klein, B.E. and Linton, K.L. (1992) Prevalence of age-related maculopathy. The Beaver Dam Eye Study. Ophthalmology, **99**, 933–943.
3. Congdon, N., O'Colmain, B., Klaver, C.C., Klein, R., Munoz, B., Friedman, D.S., Kempen, J., Taylor, H.R. and Mitchell, P. (2004) Causes and prevalence of visual impairment among adults in the United States. *Arch. Ophthalmol.*, **122**, 477–485.
4. Friedman, D.S., O'Colmain, B.J., Munoz, B., Tomany, S.C., McCarty, C., de Jong, P.T., Nemesure, B., Mitchell, P. and Kempen, J. (2004) Prevalence of age-related macular degeneration in the United States. *Arch. Ophthalmol.*, **122**, 564–572.
5. Klein, R., Peto, T., Bird, A. and Vannewkirk, M.R. (2004) The epidemiology of age-related macular degeneration. *Am. J. Ophthalmol.*, **137**, 486–495.
6. Swaroop, A., Chew, E.Y., Rickman, C.B. and Abecasis, G.R. (2009) Unraveling a multifactorial late-onset disease: from genetic susceptibility to disease mechanisms for age-related macular degeneration. *Annu. Rev. Genomics Hum. Genet.*, **10**, 19–43.
7. Miller, J.W. (2013) Age-related macular degeneration revisited – piecing the puzzle: the LXIX Edward Jackson memorial lecture. *Am. J. Ophthalmol.*, **155**, 1.e13–35.e13.
8. Jager, R.D., Mieler, W.F. and Miller, J.W. (2008) Age-related macular degeneration. *N. Engl. J. Med.*, **358**, 2606–2617.
9. Klein, R., Cruickshanks, K.J., Nash, S.D., Krantz, E.M., Nieto, F.J., Huang, G.H., Pankow, J.S. and Klein, B.E. (2010) The prevalence of age-related macular degeneration and associated risk factors. *Arch. Ophthalmol.*, **128**, 750–758.
10. Seddon, J.M., Reynolds, R., Yu, Y., Daly, M.J. and Rosner, B. (2011) Risk models for progression to advanced age-related macular degeneration using demographic, environmental, genetic, and ocular factors. *Ophthalmology*, **118**, 2203–2211.
11. Fritsche, L.G., Chen, W., Schu, M., Yaspan, B.L., Yu, Y., Thorleifsson, G., Zack, D.J., Arakawa, S., Cipriani, V., Ripke, S. *et al.* (2013) Seven new loci associated with age-related macular degeneration. *Nat. Genet.*, **45**, 433–439.
12. Klein, R.J., Zeiss, C., Chew, E.Y., Tsai, J.Y., Sackler, R.S., Haynes, C., Henning, A.K., SanGiovanni, J.P., Mane, S.M., Mayne, S.T. *et al.* (2005) Complement factor H polymorphism in age-related macular degeneration. *Science*, **308**, 385–389.
13. Edwards, A.O., Ritter, R. III, Abel, K.J., Manning, A., Panhuysen, C. and Farrer, L.A. (2005) Complement factor H polymorphism and age-related macular degeneration. *Science*, **308**, 421–424.
14. Haines, J.L. (2005) Complement factor H variant increases the risk of age-related macular degeneration. *Science*, **308**, 419–421.
15. Hageman, G.S., Anderson, D.H., Johnson, L.V., Hancox, L.S., Taiber, A.J., Hardisty, L.I., Hageman, J.L., Stockman, H.A., Borchardt, J.D., Gehrs, K.M. *et al.* (2005) A common haplotype in the complement regulatory gene factor H (HF1/CFH) predisposes individuals to age-related macular degeneration. *Proc. Natl Acad. Sci. USA*, **102**, 7227–7232.
16. Zareparsi, S., Branham, K.E., Li, M., Shah, S., Klein, R.J., Ott, J., Hoh, J., Abecasis, G.R. and Swaroop, A. (2005) Strong association of the Y402H variant in complement factor H at 1q32 with susceptibility to age-related macular degeneration. *Am. J. Hum. Genet.*, **77**, 149–153.
17. Gold, B. (2006) Variation in factor B (BF) and complement component 2 (C2) genes is associated with age-related macular degeneration. *Nat. Genet.*, **38**, 458–462.
18. Yates, J.R. (2007) Complement C3 variant and the risk of age-related macular degeneration. *N. Engl. J. Med.*, **357**, 553–561.
19. Spencer, K.L., Hauser, M.A., Olson, L.M., Schmidt, S., Scott, W.K., Gallins, P., Agarwal, A., Postel, E.A., Pericak-Vance, M.A. and Haines, J.L. (2008) Deletion of CFHR3 and CFHR1 genes in age-related macular degeneration. *Hum. Mol. Genet.*, **17**, 971–977.
20. Maller, J.B. (2007) Variation in complement factor 3 is associated with risk of age-related macular degeneration. *Nat. Genet.*, **39**, 1200–1201.
21. Francis, P.J., Hamon, S.C., Ott, J., Weleber, R.G. and Klein, M.L. (2009) Polymorphisms in C2, CFB and C3 are associated with progression to advanced age related macular degeneration associated with visual loss. *J. Med. Genet.*, **46**, 300–307.
22. Stanton, C.M., Yates, J.R., den Hollander, A.I., Seddon, J.M., Swaroop, A., Stambolian, D., Fauser, S., Hoyng, C., Yu, Y., Atsuhiro, K. *et al.* (2011) Complement factor D in age-related macular degeneration. *Invest. Ophthalmol. Vis. Sci.*, **52**, 8828–8834.
23. Hughes, A.E., Mullan, G.M. and Bradley, D.T. (2011) Complement factor B polymorphism 32W protects against age-related macular degeneration. *Mol. Vis.*, **17**, 983–988.
24. Ricklin, D., Hajishengallis, G., Yang, K. and Lambris, J.D. (2010) Complement: a key system for immune surveillance and homeostasis. *Nat. Immunol.*, **11**, 785–797.
25. Ricklin, D. and Lambris, J.D. (2013) Complement in immune and inflammatory disorders: pathophysiological mechanisms. *J. Immunol.*, **190**, 3831–3838.
26. Chi, Z.L., Yoshida, T., Lambris, J.D. and Iwata, T. (2010) Suppression of drusen formation by compstatin, a peptide inhibitor of complement C3 activation, on cynomolgus monkey with early-onset macular degeneration. *Adv. Exp. Med. Biol.*, **703**, 127–135.
27. Hageman, G.S., Luthert, P.J., Victor Chong, N.H., Johnson, L.V., Anderson, D.H. and Mullins, R.F. (2001) An integrated hypothesis that considers drusen as biomarkers of immune-mediated processes at the RPE-Bruch's membrane interface in aging and age-related macular degeneration. *Prog. Retin. Eye Res.*, **20**, 705–732.
28. Anderson, D.H., Mullins, R.F., Hageman, G.S. and Johnson, L.V. (2002) A role for local inflammation in the formation of drusen in the aging eye. *Am. J. Ophthalmol.*, **134**, 411–431.
29. Ricklin, D. and Lambris, J.D. (2013) Progress and trends in complement therapeutics. *Adv. Exp. Med. Biol.*, **735**, 1–22.
30. Ricklin, D. and Lambris, J.D. (2013) Complement in immune and inflammatory disorders: therapeutic interventions. *J. Immunol.*, **190**, 3839–3847.
31. Abdelsalam, A., Del Priore, L. and Zarbin, M.A. (1999) Drusen in age-related macular degeneration: pathogenesis, natural course, and laser photocoagulation-induced regression. *Surv. Ophthalmol.*, **44**, 1–29.
32. Bressler, N.M., Silva, J.C., Bressler, S.B., Fine, S.L. and Green, W.R. (1994) Clinicopathologic correlation of drusen and retinal pigment epithelial abnormalities in age-related macular degeneration. *Retina*, **14**, 130–142.
33. Sarks, S.H. (1976) Ageing and degeneration in the macular region: a clinico-pathological study. *Br. J. Ophthalmol.*, **60**, 324–341.
34. Sarks, S.H. (1982) Drusen patterns predisposing to geographic atrophy of the retinal pigment epithelium. *Aust. J. Ophthalmol.*, **10**, 91–97.
35. Green, W.R. and Enger, C. (1993) Age-related macular degeneration histopathologic studies. The 1992 Lorenz E. Zimmerman Lecture. *Ophthalmology*, **100**, 1519–1535.
36. Mullins, R.F., Aptsiauri, N. and Hageman, G.S. (2001) Structure and composition of drusen associated with glomerulonephritis: implications for the role of complement activation in drusen biogenesis. *Eye (London)*, **15**, 390–395.
37. Mullins, R.F., Russell, S.R., Anderson, D.H. and Hageman, G.S. (2000) Drusen associated with aging and age-related macular degeneration contain proteins common to extracellular deposits associated with atherosclerosis, elastosis, amyloidosis, and dense deposit disease. *FASEB J.*, **14**, 835–846.
38. Luibl, V., Isas, J.M., Kayed, R., Glabe, C.G., Langen, R. and Chen, J. (2006) Drusen deposits associated with aging and age-related macular degeneration contain nonfibrillar amyloid oligomers. *J. Clin. Invest.*, **116**, 378–385.
39. Crabb, J.W., Miyagi, M., Gu, X., Shadrach, K., West, K.A., Sakaguchi, H., Kamei, M., Hasan, A., Yan, L., Rayborn, M.E. *et al.* (2002) Drusen proteome analysis: an approach to the etiology of age-related macular degeneration. *Proc. Natl Acad. Sci. USA*, **99**, 14682–14687.
40. Malek, G., Li, C.M., Guidry, C., Medeiros, N.E. and Curcio, C.A. (2003) Apolipoprotein B in cholesterol-containing drusen and basal deposits of human eyes with age-related maculopathy. *Am. J. Pathol.*, **162**, 413–425.
41. Anderson, D.H., Talaga, K.C., Rivest, A.J., Barron, E., Hageman, G.S. and Johnson, L.V. (2004) Characterization of beta amyloid assemblies in drusen: the deposits associated with aging and age-related macular degeneration. *Exp. Eye Res.*, **78**, 243–256.
42. Curcio, C.A., Presley, J.B., Malek, G., Medeiros, N.E., Avery, D.V. and Kruth, H.S. (2005) Esterified and unesterified cholesterol in drusen and basal deposits of eyes with age-related maculopathy. *Exp. Eye Res.*, **81**, 731–741.
43. Curcio, C.A., Presley, J.B., Millican, C.L. and Medeiros, N.E. (2005) Basal deposits and drusen in eyes with age-related maculopathy: evidence for solid lipid particles. *Exp. Eye Res.*, **80**, 761–775.

44. Lengyel, I., Flinn, J.M., Peto, T., Linkous, D.H., Cano, K., Bird, A.C., Lanzirotti, A., Frederickson, C.J. and van Kuijk, F.J. (2007) High concentration of zinc in sub-retinal pigment epithelial deposits. *Exp. Eye Res.*, **84**, 772–780.
45. Wang, L., Clark, M.E., Crossman, D.K., Kojima, K., Messinger, J.D., Mobley, J.A. and Curcio, C.A. (2010) Abundant lipid and protein components of drusen. *PLoS ONE*, **5**, e10329.
46. Curcio, C.A. and Johnson, M. (2013) Structure, function, and pathology of Bruch's membrane. In: Ryan, S.J., Schachat, A.P., Wilkinson, C.P., Hinton, D.R., Sadda, S. and Wiedemann, P. (eds.), *Retina, 1*. Elsevier, London, pp. 466–481.
47. Anderson, D.H., Ozaki, S., Nealon, M., Neitz, J., Mullins, R.F., Hageman, G.S. and Johnson, L.V. (2001) Local cellular sources of apolipoprotein E in the human retina and retinal pigmented epithelium: implications for the process of drusen formation. *Am. J. Ophthalmol.*, **131**, 767–781.
48. Curcio, C.A. and Millican, C.L. (1999) Basal linear deposit and large drusen are specific for early age-related maculopathy. *Arch. Ophthalmol.*, **117**, 329–339.
49. Spraul, C.W., Lang, G.E., Grossniklaus, H.E. and Lang, G.K. (1999) Histologic and morphometric analysis of the choroid, Bruch's membrane, and retinal pigment epithelium in postmortem eyes with age-related macular degeneration and histologic examination of surgically excised choroidal neovascular membranes. *Surv. Ophthalmol.*, **44**(Suppl. 1), S10–S32.
50. Sarks, S., Cherepanoff, S., Killingsworth, M. and Sarks, J. (2007) Relationship of Basal laminar deposit and membranous debris to the clinical presentation of early age-related macular degeneration. *Invest. Ophthalmol. Vis. Sci.*, **48**, 968–977.
51. Kliffen, M., Mooy, C.M., Luider, T.M. and de Jong, P.T. (1994) Analysis of carbohydrate structures in basal laminar deposit in aging human maculae. *Invest. Ophthalmol. Vis. Sci.*, **35**, 2901–2905.
52. Knupp, C., Amin, S.Z., Munro, P.M., Luthert, P.J. and Squire, J.M. (2002) Collagen VI assemblies in age-related macular degeneration. *J. Struct. Biol.*, **139**, 181–189.
53. Fujihara, M., Bartels, E., Nielsen, L.B. and Handa, J.T. (2009) A human apoB100 transgenic mouse expresses human apoB100 in the RPE and develops features of early AMD. *Exp. Eye Res.*, **88**, 1115–1123.
54. Rakoczy, E.P., Yu, M.J., Nusinowitz, S., Chang, B. and Heckenlively, J.R. (2006) Mouse models of age-related macular degeneration. *Exp. Eye Res.*, **82**, 741–752.
55. Rakoczy, P.E., Zhang, D., Robertson, T., Barnett, N.L., Papadimitriou, J., Constable, I.J. and Lai, C.M. (2002) Progressive age-related changes similar to age-related macular degeneration in a transgenic mouse model. *Am. J. Pathol.*, **161**, 1515–1524.
56. Fu, L., Garland, D., Yang, Z., Shukla, D., Rajendran, A., Pearson, E., Stone, E.M., Zhang, K. and Pierce, E.A. (2007) The R345W mutation in EFEMP1 is pathogenic and causes AMD-like deposits in mice. *Hum. Mol. Genet.*, **16**, 2411–2422.
57. Marmorstein, L.Y., Munier, F.L., Arsenijevic, Y., Schorderet, D.F., McLaughlin, P.J., Chung, D., Traboulsi, E. and Marmorstein, A.D. (2002) Aberrant accumulation of EFEMP1 underlies drusen formation in Malattia Leventinese and age-related macular degeneration. *Proc. Natl Acad. Sci. USA*, **99**, 13067–13072.
58. Marmorstein, L.Y., McLaughlin, P.J., Peachey, N.S., Sasaki, T. and Marmorstein, A.D. (2007) Formation and progression of sub-retinal pigment epithelium deposits in Efemp1 mutation knock-in mice: a model for the early pathogenic course of macular degeneration. *Hum. Mol. Genet.*, **16**, 2423–2432.
59. Ramkumar, H.L., Zhang, J. and Chan, C.C. (2010) Retinal ultrastructure of murine models of dry age-related macular degeneration (AMD). *Prog. Retin. Eye Res.*, **29**, 169–190.
60. Piguet, B., Haimovici, R. and Bird, A.C. (1995) Dominantly inherited drusen represent more than one disorder: a historical review. *Eye (London)*, **9**, 34–41.
61. Stone, E.M., Braun, T.A., Russell, S.R., Kuehn, M.H., Lotery, A.J., Moore, P.A., Eastman, C.G., Casavant, T.L. and Sheffield, V.C. (2004) Missense variations in the fibulin 5 gene and age-related macular degeneration. *N. Engl. J. Med.*, **351**, 346–353.
62. Michaelides, M., Jenkins, S.A., Brantley, M.A. Jr., Andrews, R.M., Waseem, N., Luong, V., Gregory-Evans, K., Bhattacharya, S.S., Fitzke, F.W. and Webster, A.R. (2006) Maculopathy due to the R345W substitution in fibulin-3: distinct clinical features, disease variability, and extent of retinal dysfunction. *Invest. Ophthalmol. Vis. Sci.*, **47**, 3085–3097.
63. Stone, E.M., Lotery, A.J., Munier, F.L., Heon, E., Piguet, B., Guymer, R.H., Vandenburgh, K., Cousin, P., Nishimura, D., Swiderski, R.E. *et al.* (1999) A single EFEMP1 mutation associated with both Malattia Leventinese and Doyne honeycomb retinal dystrophy. *Nat. Genet.*, **22**, 199–202.
64. Giltay, R., Timpl, R. and Kostka, G. (1999) Sequence, recombinant expression and tissue localization of two novel extracellular matrix proteins, fibulin-3 and fibulin-4. *Matrix Biol.*, **18**, 469–480.
65. Timpl, R., Sasaki, T., Kostka, G. and Chu, M.L. (2003) Fibulins: a versatile family of extracellular matrix proteins. *Nat. Rev. Mol. Cell Biol.*, **4**, 479–489.
66. Kobayashi, N., Kostka, G., Garbe, J.H., Keene, D.R., Bachinger, H.P., Hanisch, F.G., Markova, D., Tsuda, T., Timpl, R., Chu, M.L. *et al.* (2007) A comparative analysis of the fibulin protein family. Biochemical characterization, binding interactions, and tissue localization. *J. Biol. Chem.*, **282**, 11805–11816.
67. Zhang, Y. and Marmorstein, L.Y. (2010) Focus on molecules: fibulin-3 (EFEMP1). *Exp. Eye Res.*, **90**, 374–375.
68. Blackburn, J., Tarttelin, E.E., Gregory-Evans, C.Y., Moosajee, M. and Gregory-Evans, K. (2003) Transcriptional regulation and expression of the dominant drusen gene FBLN3 (EFEMP1) in mammalian retina. *Invest. Ophthalmol. Vis. Sci.*, **44**, 4613–4621.
69. McLaughlin, P.J., Bakall, B., Choi, J., Liu, Z., Sasaki, T., Davis, E.C., Marmorstein, A.D. and Marmorstein, L.Y. (2007) Lack of fibulin-3 causes early aging and herniation, but not macular degeneration in mice. *Hum. Mol. Genet.*, **16**, 3059–3070.
70. Camaj, P., Seeliger, H., Ischenko, I., Krebs, S., Blum, H., De Toni, E.N., Faktorova, D., Jauch, K.W. and Bruns, C.J. (2009) EFEMP1 Binds the EGF receptor and activates MAPK and Akt pathways in pancreatic carcinoma cells. *J. Biol. Chem.*, **390**, 1293–1302.
71. Hu, B., Thirtamara-Rajamani, K.K., Sim, H. and Viapiano, M.S. (2009) Fibulin-3 is uniquely upregulated in malignant gliomas and promotes tumor cell motility and invasion. *Mol. Cancer Res.*, **7**, 1756–1770.
72. Hu, Y., Pioli, P.D., Siegel, E., Zhang, Q., Nelson, J., Chaturbedi, A., Mathews, M.S., Ro, D.I., Alkafeef, S., Hsu, N. *et al.* (2011) EFEMP1 Suppresses malignant glioma growth and exerts its action within the tumor extracellular compartment. *Mol. Cancer*, **10**, 123–135.
73. Klenotic, P.A., Munier, F.L., Marmorstein, L.Y. and Anand-Apte, B. (2004) Tissue inhibitor of metalloproteinases-3 (TIMP-3) is a binding partner of epithelial growth factor-containing fibulin-like extracellular matrix protein 1 (EFEMP1). Implications for macular degenerations. *J. Biol. Chem.*, **279**, 30469–30473.
74. Weber, B.H., Vogt, G., Pruett, R.C., Stohr, H. and Felbor, U. (1994) Mutations in the tissue inhibitor of metalloproteinases-3 (TIMP3) in patients with Sorsby's fundus dystrophy. *Nat. Genet.*, **8**, 352–356.
75. Florens, L., Carozza, M.J., Swanson, S.K., Fournier, M., Coleman, M.K., Workman, J.L. and Washburn, M.P. (2006) Analyzing chromatin remodeling complexes using shotgun proteomics and normalized spectral abundance factors. *Methods*, **40**, 303–311.
76. Liu, Q., Tan, G., Levenkova, N., Li, T., Pugh, E.N. Jr, Rux, J.J., Speicher, D.W. and Pierce, E.A. (2007) The proteome of the mouse photoreceptor sensory cilium complex. *Mol. Cell. Proteomics*, **6**, 1299–1317.
77. Hynes, R.O. (2009) The extracellular matrix: not just pretty fibrils. *Science*, **326**, 1216–1219.
78. Hynes, R.O. and Naba, A. (2012) Overview of the matrisome – an inventory of extracellular matrix constituents and functions. *Cold Spring Harb. Perspect. Biol.*, **4**, a004903.
79. Reiser, K., McCormick, R.J. and Rucker, R.B. (1992) Enzymatic and nonenzymatic cross-linking of collagen and elastin. *FASEB J.*, **6**, 2439–2449.
80. Wold, S., Esbensen, K. and Geladi, P. (1987) Principal component analysis. *Chemometr. Intell. Lab. Syst.* **2**, 37–52.
81. Abdi, H. and Williams, L.J. (2010) Principal component analysis. *Wiley Interdiscip. Rev. Comput. Stat.*, **2**, 433–459.
82. Verhoeckx, K.C., Bijlsma, S., de Groene, E.M., Witkamp, R.F., van der Greef, J. and Rodenburg, R.J. (2004) A combination of proteomics, principal component analysis and transcriptomics is a powerful tool for the identification of biomarkers for macrophage maturation in the U937 cell line. *Proteomics*, **4**, 1014–1028.
83. Rao, P.K. and Li, Q. (2009) Principal component analysis of proteome dynamics in iron-starved mycobacterium tuberculosis. *J. Proteomics Bioinform.*, **2**, 19–31.
84. Everitt, B.S., Landau, S., Leese, M. and Stahl, D. (2011) *In Cluster Analysis*, 5th edn. John Wiley & Sons, Ltd, Chichester, UK.

85. Anderson, D.W., Kish, L. and Cornell, R.G. (1980) On stratification, grouping, and matching. *Scand. J. Stat.*, **7**, 61–66.
86. Mi, H., Muruganujan, A. and Thomas, P.D. (2013) PANTHER in 2013: modeling the evolution of gene function, and other gene attributes, in the context of phylogenetic trees. *Nucleic Acids Res.*, **41**, D377–D386.
87. Eppig, J.T., Blake, J.A., Bult, C.J., Kadin, J.A. and Richardson, J.E. (2012) The mouse genome database (MGD): comprehensive resource for genetics and genomics of the laboratory mouse. *Nucleic Acids Res.*, **40**, D881–D886.
88. Sharma, M., Naslavsky, N. and Caplan, S. (2008) A role for EHD4 in the regulation of early endosomal transport. *Traffic*, **9**, 995–1018.
89. Pearse, B.M. (1976) Clathrin: a unique protein associated with intracellular transfer of membrane by coated vesicles. *Proc. Natl Acad. Sci. USA*, **73**, 1255–1259.
90. Old, W.M., Meyer-Arendt, K., Aveline-Wolf, L., Pierce, K.G., Mendoza, A., Sevinsky, J.R., Resing, K.A. and Ahn, N.G. (2005) Comparison of label-free methods for quantifying human proteins by shotgun proteomics. *Mol. Cell Proteomics*, **4**, 1487–1502.
91. Walport, M.J. (2001) Complement. Second of two parts. *N. Engl. J. Med.*, **344**, 1140–1144.
92. Walport, M.J. (2001) Complement. First of two parts. *N. Engl. J. Med.*, **344**, 1058–1066.
93. Chonn, A., Cullis, P.R. and Devine, D.V. (1991) The role of surface charge in the activation of the classical and alternative pathways of complement by liposomes. *J. Immunol.*, **146**, 4234–4241.
94. Thurman, J.M. and Holers, V.M. (2006) The central role of the alternative complement pathway in human disease. *J. Immunol.*, **176**, 1305–1310.
95. Johnson, L.V., Forest, D.L., Banna, C.D., Radeke, C.M., Maloney, M.A., Hu, J., Spencer, C.N., Walker, A.M., Tsie, M.S., Bok, D. *et al.* (2011) Cell culture model that mimics drusen formation and triggers complement activation associated with age-related macular degeneration. *Proc. Natl Acad. Sci. USA*, **108**, 18277–18282.
96. Tack, B.F., Harrison, R.A., Janatova, J., Thomas, M.L. and Prahl, J.W. (1980) Evidence for presence of an internal thiolester bond in third component of human complement. *Proc. Natl Acad. Sci. USA*, **77**, 5764–5768.
97. Harrison, R.A., Thomas, M.L. and Tack, B.F. (1981) Sequence determination of the thiolester site of the fourth component of human complement. *Proc. Natl Acad. Sci. USA*, **78**, 7388–7392.
98. Hostetter, M.K., Krueger, R.A. and Schmeling, D.J. (1984) The biochemistry of opsonization: central role of the reactive thiolester of the third component of complement. *J. Infect. Dis.*, **150**, 653–661.
99. Law, S.K. and Dodds, A.W. (1997) The internal thioester and the covalent binding properties of the complement proteins C3 and C4. *Protein Sci.*, **6**, 263–274.
100. Chong, N.H., Keonin, J., Luthert, P.J., Frennesson, C.I., Weingeist, D.M., Wolf, R.L., Mullins, R.F. and Hageman, G.S. (2005) Decreased thickness and integrity of the macular elastic layer of Bruch's membrane correspond to the distribution of lesions associated with age-related macular degeneration. *Am. J. Pathol.*, **166**, 241–251.
101. Booij, J.C., Baas, D.C., Beisekeeva, J., Gorgels, T.G. and Bergen, A.A. (2010) The dynamic nature of Bruch's membrane. *Prog. Retin. Eye. Res.*, **29**, 1–18.
102. Hayward, C., Shu, X., Cideciyan, A.V., Lennon, A., Barran, P., Zareparsi, S., Sawyer, L., Hendry, G., Dhillon, B., Milam, A.H. *et al.* (2003) Mutation in a short-chain collagen gene, CTRP5, results in extracellular deposit formation in late-onset retinal degeneration: a genetic model for age-related macular degeneration. *Hum. Mol. Genet.*, **12**, 2657–2667.
103. Chavali, V.R., Khan, N.W., Cukras, C.A., Bartsch, D.U., Jablonski, M.M. and Ayyagari, R. (2011) A CTRP5 gene S163R mutation knock-in mouse model for late-onset retinal degeneration. *Hum. Mol. Genet.*, **20**, 2000–2014.
104. Roybal, C.N., Marmorstein, L.Y., Vander Jagt, D.L. and Abcouwer, S.F. (2005) Aberrant accumulation of fibulin-3 in the endoplasmic reticulum leads to activation of the unfolded protein response and VEGF expression. *Invest. Ophthalmol. Vis. Sci.*, **46**, 3973–3979.
105. Hulleman, J.D., Kaushal, S., Balch, W.E. and Kelly, J.W. (2011) Compromised mutant EFEMP1 secretion associated with macular dystrophy remedied by proteostasis network alteration. *Mol. Biol. Cell*, **22**, 4765–4775.
106. Lawler, J. (1986) The structural and functional properties of thrombospondin. *Blood*, **67**, 1197–1209.
107. Lawler, J. (2000) The functions of thrombospondin-1 and-2. *Curr. Opin. Cell Biol.*, **12**, 634–640.
108. Lawler, J. (2002) Thrombospondin-1 as an endogenous inhibitor of angiogenesis and tumor growth. *J. Cell. Mol. Med.*, **6**, 1–12.
109. Miyajima-Uchida, H., Hayashi, H., Beppu, R., Kuroki, M., Fukami, M., Arakawa, F., Tomita, Y. and Oshima, K. (2000) Production and accumulation of thrombospondin-1 in human retinal pigment epithelial cells. *Invest. Ophthalmol. Vis. Sci.*, **41**, 561–567.
110. Wang, S., Wu, Z., Sorenson, C.M., Lawler, J. and Sheibani, N. (2003) Thrombospondin-1-deficient mice exhibit increased vascular density during retinal vascular development and are less sensitive to hyperoxia-mediated vessel obliteration. *Dev. Dyn.*, **228**, 630–642.
111. Wang, S., Sorenson, C.M. and Sheibani, N. (2012) Lack of thrombospondin 1 and exacerbation of choroidal neovascularization. *Arch. Ophthalmol.*, **130**, 615–620.
112. Uno, K., Bhutto, I.A., McLeod, D.S., Merges, C. and Lutty, G.A. (2006) Impaired expression of thrombospondin-1 in eyes with age related macular degeneration. *Br. J. Ophthalmol.*, **90**, 48–54.
113. Henkin, J. and Volpert, O.V. (2011) Therapies using anti-angiogenic peptide mimetics of thrombospondin-1. *Expert Opin. Ther. Targets*, **15**, 1369–1386.
114. He, S., Incardona, F., Jin, M., Ryan, S.J. and Hinton, D.R. (2006) Thrombospondin-1 expression in RPE and choroidal neovascular membranes. *Yan Ke Xue Bao*, **22**, 265–274.
115. Nandrot, E.F., Anand, M., Almeida, D., Atabai, K., Sheppard, D. and Finnemann, S.C. (2007) Essential role for MFG-E8 as ligand for alphavbeta5 integrin in diurnal retinal phagocytosis. *Proc. Natl Acad. Sci. USA*, **104**, 12005–12010.
116. Atabai, K., Jame, S., Azhar, N., Kuo, A., Lam, M., McKleroy, W., Dehart, G., Rahman, S., Xia, D.D., Melton, A.C. *et al.* (2009) Mfge8 diminishes the severity of tissue fibrosis in mice by binding and targeting collagen for uptake by macrophages. *J. Clin. Invest.*, **119**, 3713–3722.
117. Engvall, E., Hessle, H. and Klier, G. (1986) Molecular assembly, secretion, and matrix deposition of type VI collagen. *J. Cell Biol.*, **102**, 703–710.
118. Bidanset, D.J., Guidry, C., Rosenberg, L.C., Choi, H.U., Timpl, R. and Hook, M. (1992) Binding of the proteoglycan decorin to collagen type VI. *J. Biol. Chem.*, **267**, 5250–5256.
119. Danielson, K.G., Baribault, H., Holmes, D.F., Graham, H., Kadler, K.E. and Iozzo, R.V. (1997) Targeted disruption of decorin leads to abnormal collagen fibril morphology and skin fragility. *J. Cell Biol.*, **136**, 729–743.
120. Wiberg, C., Heinegard, D., Wenglen, C., Timpl, R. and Morgelin, M. (2002) Biglycan organizes collagen VI into hexagonal-like networks resembling tissue structures. *J. Biol. Chem.*, **277**, 49120–49126.
121. Chong, N.H., Alexander, R.A., Gin, T., Bird, A.C. and Luthert, P.J. (2000) TIMP-3, collagen, and elastin immunohistochemistry and histopathology of Sorsby's fundus dystrophy. *Invest. Ophthalmol. Vis. Sci.*, **41**, 898–902.
122. Knupp, C., Chong, N.H., Munro, P.M., Luthert, P.J. and Squire, J.M. (2002) Analysis of the collagen VI assemblies associated with Sorsby's fundus dystrophy. *J. Struct. Biol.*, **137**, 31–40.
123. Kuo, H.J., Keene, D.R. and Glanville, R.W. (1995) The macromolecular structure of type-VI collagen. Formation and stability of filaments. *Eur. J. Biochem.*, **232**, 364–372.
124. Reale, E., Groos, S., Luciano, L., Eckardt, C. and Eckardt, U. (2001) In the mammalian eye type VI collagen tetramers form three morphologically different aggregates. *Matrix Biol.*, **20**, 37–51.
125. Yuan, X., Gu, X., Crabb, J.S., Yue, X., Shadrach, K., Hollyfield, J.G. and Crabb, J.W. (2010) Quantitative proteomics: comparison of the macular Bruch membrane/choroid complex from age-related macular degeneration and normal eyes. *Mol. Cell. Proteomics*, **9**, 1031–1046.
126. Circolo, A., Garnier, G., Fukuda, W., Wang, X., Hidvegi, T., Szalai, A.J., Briles, D.E., Volanakis, J.E., Wetsel, R.A. and Colten, H.R. (1999) Genetic disruption of the murine complement C3 promoter region generates deficient mice with extrahepatic expression of C3 mRNA. *Immunopharmacology*, **42**, 135–149.
127. Schneider, C.A., Rasband, W.S. and Eliceiri, K.W. (2012) NIH image to ImageJ: 25 years of image analysis. *Nat. Methods*, **9**, 671–675.
128. Culp, W.D., Neal, R., Massey, R., Egevad, L., Pisa, P. and Garland, D. (2006) Proteomic analysis of tumor establishment and growth in the B16-F10 mouse melanoma model. *J. Proteome Res.*, **5**, 1332–1343.